Loading-rate Dependant Fracture Behavior of Cemented Paste Backfill under Curing Pressure

By

Tyler Runions

A thesis submitted to the Faculty of Graduate Studies in partial fulfillment of the requirements for the Degree of Master of Science

in Civil Engineering

Supervisor: **Dr. Liang Cui**

Associate Professor – Dept. of Civil Engineering

Lakehead University Thunder Bay, Ontario August 2025

Author’s Declaration Page

I hereby declare that I am the sole author of this thesis. This is a true copy of the thesis, including any required final revisions, as accepted by my examiners. I understand that my thesis may be made electronically available to the public.

Abstract

This study investigates the loading-rate-dependent fracture behavior of cemented paste backfill (CPB) under varying curing pressures. CPB is widely used in underground mining to fill voids, and its mechanical performance is critical to ground stability and operational safety. While most laboratory testing is conducted under atmospheric conditions, CPB in the field cures under confining pressure, which can significantly affect its mechanical properties. To simulate real-world conditions, CPB samples were prepared and cured at pressures of 0, 29, and 58 psi, representing different backfill heights. Samples were tested at 7-, 28-, and 90-days using fracture mechanics-based tests under three different loading rates (0.1, 1, and 10 mm/min) across Mode I, II, and III fracture modes. Key parameters examined included material stiffness, fracture toughness, energy of crack initiation, and total energy of fracture.

The results demonstrated that both higher curing pressure and increased loading rate generally enhance the mechanical performance of CPB, with the most significant gains observed between 0.1 and 1 mm/min. Notably, stiffness and fracture toughness improved with curing time, while energy absorption was primarily governed by crack initiation. Auxiliary testing confirmed that increased curing pressure led to denser microstructure, slightly lower void ratios, and higher degrees of saturation. These physical changes likely contributed to the enhanced fracture behavior. The findings underscore the importance of considering both curing conditions and loading rate in the design and testing of CPB to ensure accurate predictions of field performance.

Acknowledgments

I am extremely proud to have conducted this research under the expertise and guidance of Dr. Liang Cui. The level of knowledge he posses in this field has constantly left me amazed. His willingness to both let me learn independently, and to help when I was struggling, provided the perfect balance towards developing my own knowledge in geotechnical engineering. Thank you, Dr. Cui, for allowing me this experience.

I am also very thankful for my thesis committee members, Dr. Baoqiang Liao and Dr. Jian Deng. I am grateful for their involvement in this work and strongly appreciate their valuable feedback.

I would also like to thank my family and friends for supporting and encouraging me throughout this research. They have been there throughout every difficulty I've faced, and every milestone I've achieved has been thanks to their help.

Table of contents

Contents

List of Tables and Figures

Tables

Figures

List of Equations

Abbreviations

CBM	Cement-based material
CPB	Cement-paste backfill
k_m	Material stiffness (N/mm)
P	Maximum Force (N)
F_p	peak value force (N)
D	Diameter of the sample (m)
t	Thickness of sample (m)
B	Thickness of sample (m)
S	Distance between load frame support bars (m)
W	Width of the sample (m)
a	Notch length (m)
K_I	Mode-I Fracture Toughness (kPa·$m^{1/2}$)
K_{II}	Mode-II Fracture Toughness (kPa·$m^{1/2}$)
K_{III}	Mode-III Fracture Toughness (kPa·$m^{1/2}$)
Y_I	Normalized stress intensity factor for mode-I
Y_{II}	Normalized stress intensity factor for mode-II
Y_{III}	Normalized stress intensity factor for mode-III

Chapter 1 Introduction

The increasing complexity of modern engineering challenges, particularly in fields such as construction, mining, and environmental geotechnics; has heightened the need for innovative, sustainable, and efficient materials. With growing attention toward material performance under various loading and environmental conditions, research in engineered cementitious materials has expanded rapidly. Among these, specialized materials such as cement paste backfill (CPB) have drawn significant interest due to their role in underground support systems, waste management, and cost effectiveness.

This study seeks to better understand the mechanical behavior and performance of such materials under controlled laboratory conditions. Namely, it will investigate how factors such as curing pressure, loading rate, and microstructural interactions influence mechanical properties like stiffness, fracture toughness, and energy absorption. Examining how the performance of CPB is affected by the above-mentioned factors is vital for ensuring both safety and efficiency in real world applications.

The following sections in this chapter provides a foundation for the study by introducing the background and context, defining the research problem, outlining the objectives, describing the research methodology, and presenting the organization of the thesis.

1.1 Background Information

Cemented paste backfill (CPB) is an engineered cementitious material used in underground mining operations to fill voids left behind by the mining procedure. These voids are created due to the extraction of ore, and they are typically referred to as stopes.

Once a stope has been dug out, it is then backfilled before the mining operation proceeds to the next area. CPB is a material that can fill these stopes and is composed primarily of dewatered mine tailings (such as silica), a binder (usually Portland cement or other cementitious materials), and water to facilitate the hydration reaction. Once placed, the mixture hardens over time to form a solid material. The material then provides structural support to the surrounding rock, thereby enhancing ground stability and enabling safer extraction of stopes in adjacent areas.

The use of CPB addresses several critical operational and environmental concerns in the mining industry. Traditionally mine tailings are disposed of in surface tailings storage facilities or ponds - which pose risks of environmental contamination, dam failure, and long-term site management issues. CPB significantly reduces the reliance on these methods of impounding tailings by reintroducing the waste material back into the underground mine, effectively providing a recycling process. This recycling process provides numerous benefits such as lowering harmful environmental impact and reducing the volume of surface storage infrastructure required.

Economically, CPB can offer cost advantages over alternative backfilling methods. Its ability to use existing tailings materials may lower raw material and transportation costs. Furthermore, its workable nature allows for efficient placement through pipelines, reducing the need for extensive labor or mechanical placement.

Overall, the use of CPB provides a solution to geotechnical challenges, promotes environmental responsibility, and is economically efficient. This potentially makes it a great choice for many modern underground mining operations.

Backfilling materials are broadly classified into three main categories: rockfill, hydraulic fill, and paste backfill. *Rockfill* consists of coarse, well-graded rock fragments placed and compacted to provide high strength and stability; it is often used in dam construction and large retaining structures where drainage is also a key consideration. *Hydraulic fill* involves the placement of soil or tailings in a slurry form, transported hydraulically and deposited into place; while economical for large-scale operations such as mine backfilling, its mechanical performance is generally weaker unless stabilized. *Paste backfill* is how CPB can be classified. This type of backfill has gained prominence in mining and geotechnical applications because it not only provides ground support and reduces subsidence risks but also offers an effective means of tailings management.

1.2 Research Problem

The performance of cement paste backfill or other cementitious materials in an underground mining setting is influenced by a range of variables. Particularly, the loading rates the material experiences and the conditions under which it cures.

CPB may be subjected to both gradual and rapid loading due to mining activities or environmental factors, each affecting its mechanical response differently. The variance of possible loads is discussed further in chapter 2.0.

Curing pressure can also significantly influence strength development and material properties. While most lab tests are conducted under atmospheric pressure, real-world backfill cures under confined conditions, especially at depth. This mismatch can lead to inaccurate predictions of field performance.

As a result, there is a need for a better understanding of how curing pressure and loading rate interact to affect the mechanical behavior of CPB. Improving understanding of these aspects can lead to better design accuracy and backfill reliability.

1.3 Research Objectives

The objective of this research is to better understand how cement paste backfill responds to varying loading rates and curing pressures, with the aim of improving performance understanding under conditions that more closely resemble those found in underground mining environments. This study seeks to collect experimental data on the mechanical performance of CPB samples subjected to different loading and curing scenarios, in order to identify patterns or trends in strength, stiffness, and failure behavior. In addition to the primary mechanical testing, auxiliary data -such as density, moisture content, and physical observations - will be gathered to help explain any unexpected results or outliers. Together, these efforts aim to provide a more comprehensive understanding of the key variables affecting CPB performance, which can aid in future backfill design and testing practices.

1.4 Research Methodology

This study will take an experimental approach to investigate how curing pressure and loading rate influence the fracture behavior of CPB. The testing program focuses on fracture mechanics rather than traditional strength-based testing - using Mode I to Mode III loading conditions to assess crack initiation, propagation, and energy absorption. The reason this type of testing was selected is explored more in Chapters 2 and 3, but it relates to how the failure of CPB will be governed by its fracture behavior.

Samples are prepared under controlled conditions and cured at three different confining pressures: 0 psi, 29 psi, and 58 psi. Each curing condition is applied to sets of samples tested at 7, 28, and 90 days to also capture the evolution of mechanical behavior over time.

To evaluate the influence of loading rate, samples are subjected to controlled displacement during testing, and load–displacement data is collected throughout each test. This data is used to assess stiffness, fracture toughness, and energy-based properties. Auxiliary measurements and physical observations are also collected to help explain variations or outliers in the results.

A detailed description of the experimental procedures, including sample preparation, curing setups, testing configurations, and data analysis methods, is provided in Chapter 3.

1.5 Organization of Thesis

To summarize the remaining contents of this thesis, the following chapters will be composed of a literature review, an outline of the experimental testing plan, the results and analysis of the research, and then an outline of the conclusions and recommendations that can be made.

The literature review, chapter 2, will examine the fracture behavior of cementitious materials in general - especially concerning their sensitivity to different loading rates. As briefly mentioned, chapter 3 will provide a detailed overview of the experimental testing plan and methodology used to achieve it. Chapter 3 will also go into further details about why certain choices were made regarding the experimental testing. Chapter 4 will then present the results obtained from the research plan, and a data analysis based on those results. It will also provide discussion on these topics. Finally, chapter 5 will provide some conclusions that can be drawn from the research conducted in this study.

Chapter 2 Literature Review

As a construction material, cement-based materials (CBM) - such as concrete or cement paste backfill - have been widely applied to construction projects both underground and on the earth's surface. The mechanical behavior and performance of CBM's play a crucial role in their successful engineering application. The accurate, reliable assessment of mechanical behavior and properties of a CBM requires full consideration of field loading conditions.

The first type of loading that may be experienced in the field can be referred to as what is known as a service load. Service loads are typically due to the transfer of machinery or equipment over an element. In this case, the load will increase and decrease on the element as differently weighted equipment transfers force on and off it. To add to this, the rate that this load is applied may vary based on how fast the equipment passes over it. To summarize: a cement-based element may experience different magnitudes of loadings under different loading rates due to the movement of operational equipment.

These variable service loads are something critical to consider in the case of a CBM being used in a mining setting. In a mining operation, access roads will often be on top of or beside areas filled in with CBM. The movement of mining equipment over these access roads will provide different loads applied at different loading rates (Nie et al. [1]). By properly considering how service loads may be applied to CBM through different loading rates, a safer mining operation can be ensured through achieving more accurate design requirements.

Another type of loading that may be experienced in the field are loadings due to the environment. Typical examples of this include loads due to wind, seismic activity, or current. Loadings due to these events are not constant. For example, if wind were to be considered, it is known that the speed of the wind is something that changes throughout any given day. It is also known that while the speed of the wind may change, it will also change at different rates.

For the application of CBM in a mining setting, consideration of possible seismic loading would be the most important environmental load to consider. Although the sensation of an earthquake is composed of horizontal and vertical motions, the horizontal movement is what must be considered as a seismic load (Lin and Yoda [2]), as this is how seismic loads are applied to structures or underground support. Therefore, the seismic load that a structure will experience is related to the magnitude of any seismic activity it undergoes. Earthquake magnitude may vary, and furthermore, the rate at which seismic activity occurs is not constant over the course of an earthquake (Shimizu [3]). This means that as the load due to seismic activity changes, so will the loading rate of the applied seismic load. Consequently, when considering possible environmental loadings, the loading rates must also be considered similarly to how the loadings rates of service loads must be considered. Below in table 2.1, typical loading rates that may be experienced in the field can be seen:

Table 2.1 – Typical Loading Rates

Loading	Loading Rate Type	Typical Range (mm/min)	Reference
Seismic Loading	Environmental	1000-1,000,000	[4]
Blasting Vibrations	Environmental	100-500,000	[5]
Heavy Mining Equipment	Service Load	0.01-1	[6]
Light Mining Equipment	Service Load	0.001-0.1	[7]
Rock Mass Creep	Environmental	0.000001–0.001	[8]
Ground Support Activation	Service Load	0.001–0.1	[9]

Considering the types of loadings mentioned above that a CBM might be subjected to as part of an underground structure, examining how applying different loading rates to the CBM will lead to a better understanding of how the CBM will behave in the field. Due to the sensitivity of loading rate, CBM may demonstrate distinct mechanical behaviors and properties under complex field loading conditions and thus imposes significant influence on mechanical stability of CBM structures.

In terms of mechanical behaviors, the performance of CBM may improve under higher loading rates. Zhang et al. [10] found that peak loads can increase in line with increases in loading rates. This means that a higher final magnitude of loading can be expected to be reached if the load is applied faster. The peak loads that are reached under different loading rates also correspond to different values of displacement, which follow the same trend of increasing with loading rate.

Meng et al. [11] found that as the loading rate increases, the fracture energy increases non-linearly at a decreasing rate. This means that as loads are applied faster, CBM can absorb a larger amount of energy before cracks begin to form. This effect starts to fall off as the loading rate increases to higher levels. It is important to understand the cracking behavior of CBM under different loading rates to understand when the CBM will begin to fail.

Apart from the mechanical behavior, the mechanical properties of CBM also show strong dependencies on the loading rate. For instance, the elastic modulus of a CBM will come out to higher values as loading rate increase. The same can also be said about strength related parameters such as compressional strength and flexural strength. In table 2.2, a summary is provided on how various mechanical properties of different cement-based materials will change as the loading rate increases. From this table, different loading rates will result in different critical values of mechanical behavior. Hence, it is of great importance to fully understand loading rate-dependent mechanical behavior of CBM.

Table 2.2 - Summary of mechanical properties of CBM under different loading rates.

Materials	Mechanical properties	Loading Rate (mm/min)	Typical Values	Reference
Concrete	Elastic modulus (MPa)	0.01 – 0.1	20000-35000 30000-45000	[12]
	UCS (GPa)	0.5 3	20-40 40-60	[13]
	Tensile strength (GPa)	0.01-0.1 2	2-4 4-6	[14]
	Flexural strength (GPa)	0.05 2	3-6 5-8	[15]
	Fracture Toughness ($MPa*m^{1/2}$)	0.01-0.1	0.2-0.4 0.4-0.8	[16]
	Fracture energy (J/m^2)	0.1 1-3	80–150 150–300	[17]
Cemented soils	Elastic modulus (GPa)	0.1-0.5 1-5	100-300 300-800	[18]
	UCS (MPa)	0.5 2.4	0.5-2 2-4	[18]
	Tensile strength (MPa)	0.1 1	0.05-0.2 0.2-0.5	[19]
	Flexural strength (MPa)	0.05-0.2 1.5	0.1-0.3 0.3-0.7	[20]
	Fracture toughness ($MPa*m^{1/2}$)	0.2 2	0.04-0.08 0.1-0.2	[21]
	Fracture energy (J/m^2)	0.2 2	20–80 80–180	[22]
Cemented Paste Backfill	Elastic modulus (GPa)	0.25 2	200-500 500-1000	[23]
	UCS (MPa)	0.5 2	0.3-1 1-2	[24]
	Tensile strength (MPa)	0.1 1	0.03-0.1 0.1-0.4	[25]
	Flexural strength (MPa)	0.1 2	0.1-0.2 0.3-0.6	[25]
	Fracture toughness ($MPa*m^{1/2}$)	0.25 2	0.05-0.08 0.1-0.15	[26]
	Fracture energy (J/m^2)	0.25 2	20–60 100–150	[26]

Cementitious materials are one major, although small in volume, component of a cement-based material. Cementitious materials are typically small to medium in particle size and may be created with the use of different types of byproducts, such as mining tailings. Mining tailings may be utilized to form CPB – which may be composed of different oxygen-based compounds, such as quicklime (CaO) or ferric oxide (Fe_2O_3) (Lu et al. [27]). CPB can form strong structural members through the binding of aggregate materials. This is accomplished through a reaction known as hydration.

Hydration involves dissolution and precipitation, which will result in the formation of various hydrates. The formation of these hydrates is what allows the CBM to harden (Marchon and Flatt [28]). The hardening of the cementitious materials due to this reaction is what will form the strong bonds present between aggregates. After hardening, this will create the final product of a cement-based material, where the CBM will have a relatively high compressive strength and may be used to form structures.

One previously mentioned example of a cement-based material is cement paste backfill. The use of CPB specifically in a mining setting is advantageous in facilitating a recycling process since the mine waste (tailings) can be used to backfill the mine through the creation of CPB. The waste tailings are non-toxic, which means the use of cement paste to backfill a mine will not cause any environmental consequences (Lu et al. [27]). The limitations of using CPB compared to typical concrete made with Portland cement is mostly that the CPB will be weaker in strength, as seen in table 2.2.

When a cement-based mix is created, the mixture can be cast and tested to examine the mechanical behavior of the mix. This is done by applying an increasing a load and noting when the specimen fractures. The fracture toughness is an important property that can describe critical stress states about the initial fracturing of the tested specimen (Ayatollahi and Aliha [29]). CPB may be classified as a brittle material. This means that as it bears a higher loading, the material may begin to crack. When the cracks lead to complete fractures, the CPB will fail (Cui and McAdie [30]). Therefore, it is vital to understand fracture behavior since it will lead to the failure of a CPB element.

Since the fracture behavior of cementitious materials governs their engineering performance, it is of theoretical and practical importance to offer an in-depth understanding of the loading-rate-dependent behavior of cementitious materials. Therefore, the objective of this literature review is to (1) summarize the influence of loading rate on the tensile and shear crack behavior and (2) identify the mechanism responsible for the sensitivity of fracture behavior to the loading rate.

2.1 Effect of Loading Rate on Tensile Crack Behavior of Cementitious Materials

Mode-I crack behavior describes the fracture toughness of a material related to tensile crack propagation (Wu et al. [31]). It is also referred to as the tensile opening mode. When tests are carried out to examine mode-I fracture behavior, the tension cracks are induced through compression (Kuruppu et al. [32]). This is desirable, as CBM tends to be weaker in tension. The cracks that a specimen will experience through testing of this mode separate in the direction that is normal to the plane of the crack, as seen in figure 2.1 [33].

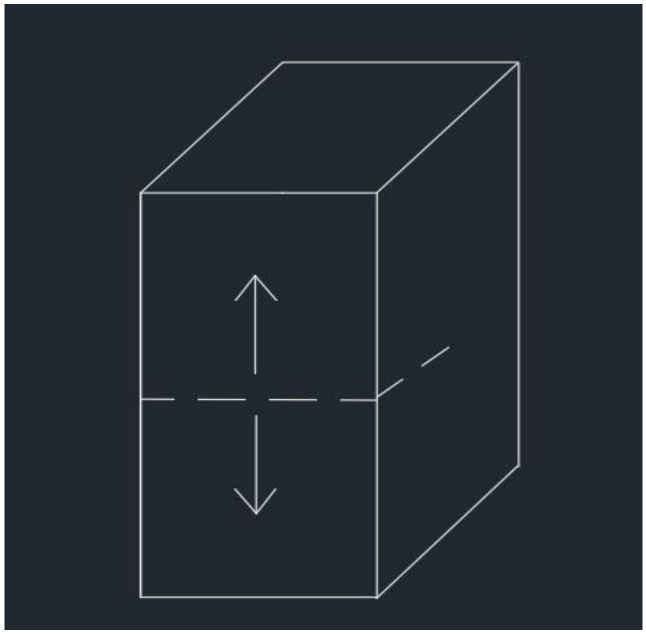

Figure 2.1: Visualization of Mode-I Crack Propagation.

One important variable to consider during a mode-I test is what the applied loading rate will be. To gain a sense of typical loading rate ranges used in mode-I related studies on CPB, a review of several previous studies and recommendations is required.

Cui and McAdie [30] conducted a study on the fracture behavior and properties of sulfate-rich fiber-reinforced CPB. For mode-I testing, SCB tests were performed at a loading rate of 1mm/min. This loading rate was held constant throughout this studies research trials, and the value was justified through several recommendations from previous studies.

Xiu et al. [34] investigated the effect of loading rate on the uniaxial compressive strength (UCS) of CPB. Although mode-I relates to tension, the tension cracks are induced through compression. Therefore, the loading rates used in this study can still be examined to gain a sense of typical loading rates applied to a CPB specimen. For this study, the range of loading rates includes: 0.1, 0.25, 0.5, 1, 2 mm/min.

Song et al. [35] completed research on the effects of the binder type, and the amount used in a CPB mix, for mode I fracture. This was done through SCB testing, with an adopted fixed loading rate of 0.5mm/min. The static loading rate used in this study is below the value used by Cui and McAdie [30], where several recommendations were followed. Although 0.5 and 1 mm/min are relatively close, this would suggest that 0.5mm/min could be said to be the start of a low loading rate range for CPB SCB mode-I testing.

Ma et al. [36] investigated the effects of loading rate on mixed mode I-II cracking in concrete. Although mixed mode I-II testing is not the same as pure mode I testing, and the material used is concrete instead of CPB, the loading rates used in this study can still be compared to what has been found so far. This study used a range of loading rates from 0.012, 0.12, 1.2, 12 and 120 mm/min. It is worth looking at this range of loading rates due to how much more extreme the lower and upper values are. 12 and especially 120mm/min are quite high rates compared to what different studies have used, while 0.012mm/min is very low comparatively.

After examining the range of loading rates adopted by researchers, loading rate values can begin to be viewed as high or low for what is commonly used. Based on the above paragraphs, a loading rate of 1mm/min can be viewed as a typical amount. When loading rates have been scaled in research, they are usually done in a logarithmic fashion (IE a study will examine what happens at 1, 100, and 1000 mm/min as opposed to just 1,2,3 mm/min).

Combining these two general findings, this would mean that typical low loading rates could be in the range of 0.001mm/min to 1mm/min, while high loading rates can be considered in the range of 1mm/min to 1000mm/min. Consequently, the difference in the development of tensile cracks between high loading rates and low loading rates should be examined to properly understand the effects of loading rates.

To examine the mode-I cracking behavior of cementitious materials related to the applied loading rate, load displacement curves from various studies may be considered. In figure 2.2, a graph of peak load vs midspan displacement can be seen. These curves are representative of the mode-I cracking behavior for a concrete CBM, under different applied loading rates.

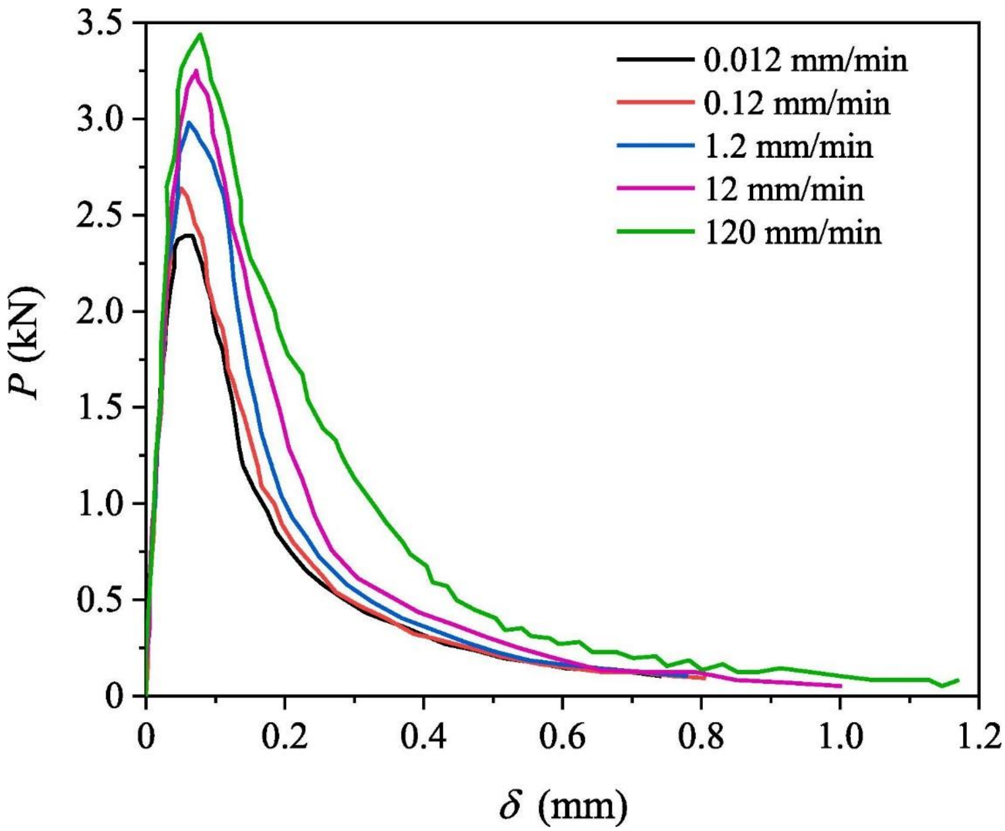

Figure 2.2: Load vs Midspan Deflection of Concrete, in Mode-I Testing (Ma et al. [36])

As can be seen from this figure, each loading rate reaches a different peak load, with the higher loading rates being able to reach larger peaks. To further discuss the behavior of concrete under this testing, the sections of the graph before and after the peak can be considered separately.

In the pre-peak portion of this graph, the material behaves similarly under each loading rate. Before the lowest peak load for a loading rate of 0.0012 mm/min is reached, the slopes for each type of loading rate are the same. This implies that a difference in loading rate has no effect on the material up until this point. The slope for each loading rate is also linear during the pre-peak portion, which implies that the material is behaving elastically. As each loading rate approaches its peak load, the slope starts to become non-linear. This is the start of the material behaving plastically – although it does not remain in this portion of the curve for very long. This implies that the material is behaving as more of a brittle material, since it does not have much capacity to elastically displace. The final thing worth noting once again is that under high loading rates, the material can reach higher peak loads. As can be seen from the figure, the material will plastically deform slightly more under higher loading rates before reaching failure at the peak load. The peak load is reached at similar displacement for all loading rates, which implies that the material is behaving stiffer at higher loading rates.

Next, the post-peak portion of the graph can be discussed. From figure 2.2, after reaching failure, the concrete still has some capacity to resist the loading. This can be referred to as the sample's residual strength. The samples with lower loading rates reach their peak load first and then demonstrate a larger slope downwards than the samples with higher loading rates as displacement continues. The area under each curve represents the energy absorbed, or work done, for a given specimen. This means that higher loading rates allow for the material to absorb more energy, especially in the post-peak portion of the curve. It is worth noting that while the slopes and areas under each curve are different in the post-peak portion, the same trend is seen for all values of loading rates. The last thing to note as well is that for higher loading rates, the material continues to have low amounts of residual strength across a longer displacement compared to when low loading rates are used.

2.2 Effect of Loading Rate on Shear Crack Behavior of Cementitious Materials

Mode-II and Mode-III crack behavior describe the fracture toughness of a material related to shear crack propagation (Saadati et al. [37]). Specifically, mode-II relates to in-plane shear, or sliding mode. A Visualization of this can be seen in Figure 2.3. Comparatively, Mode-III relates to out-of-plane shear, otherwise known as tearing mode. Another visualization is provided in figure 2.4. Similarly, to testing for mode-I behavior, the loading rate is an important parameter in mode-II and mode-III testing. To gain an understanding of typical adopted loading rates for these tests, previous studies related to CBM's can be examined.

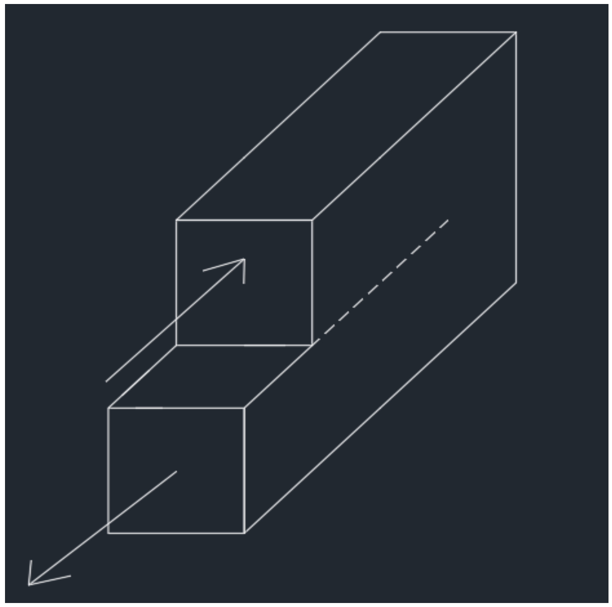

Figure 2.3: Visualization of Mode-II Crack Propagation.

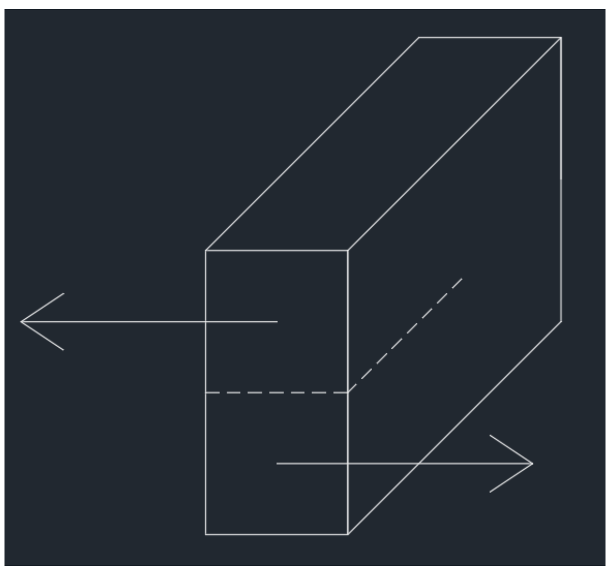

Figure 2.4: Visualization of Mode-III Crack Propagation.

Fang et al. [38] conducted research on both the mode-I and mode-II fracture toughness of CPB. Specifically, the effect of different mixes, temperatures, and chemical composition was studied. This paper chose a constant loading rate of 0.05mm/min for both mode-I and mode-II testing. Although more studies need to be conducted to gauge this loading rate as a high or low value for mode-II and III testing, the fact that the loading rate is not changed for each test is a sign that the mode-II and III loading rates may be of values in the same range.

Similarly to the above, Fang and Cui [39] carried out testing related to both mode-I and mode-II crack behavior. The adopted loading rate was 1mm/min. This was used for SCB testing of mode-I behavior, and direct shear testing for mode-II behavior. This is a second confirmation that the loading rate does not need to vary between types of testing. As 1mm/min was considered a standard loading rate in section 2; it was the rate that was the divide between what is considered high and low values. Studies by Fang et al. [38], may be indicative that the same is true.

Since all three modes were investigated by Cui and McAdie [30], the study can be examined again for adopted loading rates used in mode-II and mode-III testing. In this study, ENDB testing was conducted to study the mode-III behavior of fiber-reinforced sulfate-rich CPB. It is discussed that a typical range of loading rates for an ENDB test can range from 0.05mm/min to 5mm/min. A rate of 1mm/min was chosen to be consistent with the SCB testing performed related to mode I and II. For a third time, this concludes that the rates used in mode II and III testing are similar to mode-I testing.

Due to these findings, a rate of 1mm/min will also be chosen as a typical value for mode II and III testing. Loading rates below this value may be considered low, especially as they scale down logarithmically. Consequently, loading rates above 1mm/min may be considered high values for experimenting as they scale up similarly. Considering this range of loading rates, the fracture behavior of a CBM under mode II and mode III can be examined in existing studies.

First, when considering mode III fracture behavior, there have not been many studies conducted. It has been found that there is a significant gap in research concerning mode III fracture behavior. Mode II and mode III are more closely related to each other than to mode I however, as they both deal with shear forces. The fracture behavior of CBM under mode II in existing studies may potentially shine some light on how it may perform under mode III testing as well.

To examine the effects of loading rate on CBM under mode II loading, a study by Gao et al. [40] can be considered. Engineered cementitious composites were used for mode II testing, under 5 different loading rates. In table 2.3, a summary of their findings related to fracture toughness can be found:

Table 2.3 - Mode II Fracture Toughness vs Loading Rate

Loading Rate (mm/s)	Load Rate (mm/min)	Initial Cracking Load (kN)	Fracture Toughness ($MPa \cdot m^{1/2}$)
0.0004	0.024	10.4	0.37
0.001	0.06	11.5	0.41
0.01	0.6	14.7	0.53
0.1	6	15.4	0.55
1	60	16.4	0.60

As table 2.3 has shown, as the applied loading rate increases, there is an increase in the load that caused cracking and the fracture toughness of a sample. This coincides with the relationship between loading rate and fracture toughness from Mode I testing. The similarity in fracture toughness trends between Mode I and Mode II across loading rates suggests that the material’s rate sensitivity may be similar across all modes of testing.

2.3 Mechanisms for the Loading-rate Dependent Fracture Behavior

In this section of the literature review, possible different mechanisms that influence the fracture behavior of CBM's will be considered. This will provide insight into why the material may perform differently during tests as loading rates are increased. Doing this will also provide possible explanations for variations in testing results, and serve as a discussion tool regarding any outliers that may occur during testing.

2.3.1 Particle Interaction

The first mechanism to examine is how the material's particles will interact with each other as loading rate is changed. At higher loading rates, the interaction between particles - including cement, tailings, and any aggregates - becomes a key contributor to enhanced fracture resistance. Fast loading leaves less time for particle rearrangement or sliding, which increases the friction between interfacing particles and can provide an interlocking effect where fracture is occurring. This phenomenon has been observed in granular and cementitious systems via Discrete Element Method simulations. Momentum transfer at contacts, tangential stiffness, and coulomb friction collectively contribute to a steeper load–displacement slope and greater level of energy required to reach fracture (Nitika and Tejchman [41]).

At higher loading rates, particle interaction becomes more pronounced—boosting stiffness, peak load, and fracture energy. This aligns well with the increased fracture toughness observed experimentally and provides a micro-level mechanical basis for the rate-dependent improvement found in studies examining cracking.

2.3.2 Elastoviscosity

At elevated loading rates, cement-based materials exhibit elastoviscous behavior. This means that the viscous component of deformation - creep or stress relaxation - is suppressed, leading to both a more stiff and more elastic response. This viscoelastic coupling results in increased apparent fracture toughness, since the cracking process must overcome both elastic straining and diminished viscous dissipation. In this case, less time is available for microcrack growth or damage localization, requiring greater stress and energy input to initiate and propagate fractures (Lai and Sun [42]).

Elastoviscosity provides a well-supported mechanism explaining why fracture toughness and peak load increase with loading rate. By possibly increasing stiffness and improving the elasticity of the material, it will require higher energy input for crack propagation.

2.3.3 Inertial Effect

At high loading rates, inertial forces - arising from the resistance of the material's own mass to acceleration - begin to influence the fracture process in cement-based materials. As cracks initiate and propagate, different sections of the specimen must rapidly accelerate, particularly near the crack tip. This introduces additional resistance to deformation, since energy is now required not only to break cohesive bonds but also to overcome the inertia of the surrounding material. As a result, this increases the apparent fracture toughness and peak load (Zhang et al [43]).

Considering the above, inertial effects can play a dominant role in rate-dependent fracture toughness at high loading rates. This contributes to elevated peak load and energy dissipation beyond what would be predicted by elastic mechanisms alone.

2.3.4 Pore Water Pressure

In saturated or partially saturated CBM's, pore water pressure can significantly influence fracture behavior – especially under rapid loading. When the material is loaded quickly, there is insufficient time for pore water to drain, leading to a transient buildup of pressure within microcracks and pores. This reduces the effective stress acting on the material, which can in some cases delay crack initiation or alter crack propagation paths. This effectively increases the energy required to fracture the material (Shilko et al. [44]).

Therefore, as loading rate is increased during testing on a CBM, it is possible that the effects of the materials pore water pressure will further contribute to an increase in fracture toughness. However, at lower loading rates the pore water pressure may play a different role.

At lower or intermediate loading rates, pore water pressure can act detrimentally within microcracks and along weak interfaces in cement-based materials. Unlike the rapid loading scenario where pore water is trapped and resists crack opening, slower loading allows for partial drainage and pressure redistribution. Under these conditions, the pore water pressure may increase crack propagation by separating particle contacts and reducing the effective cohesion between solid phases. This mechanism effectively lowers the energy barrier for crack growth, leading to a reduction in fracture toughness. Experimental studies on saturated concrete and mortar have observed such behavior, finding that increased saturation or fluid presence can weaken the material's resistance to fracture under various loading conditions (Bažant and Najjar [45]).

This would imply that pore water pressure will play an important role in studying the loading rate effects on a CBM. At higher loading rates, pore water pressure may increase fracture toughness, and it may decrease fracture toughness at lower or moderate loading rates. Pore water pressure may therefore be an important mechanism in explaining any larger changes in fracture toughness as the applied loading rate to a material is increased.

2.3.5 Thermal Effect

Elevated curing temperatures significantly influence the microstructure and fracture properties of CBM's. Early exposure to high temperatures accelerates hydration, resulting in increased early-age fracture toughness and fracture energy due to denser microstructure and finer pore distribution. However, this early gain is often offset by the formation of thermal gradients and associated microcracking during cooling. These microcracks reduces long-term toughness and energy release rates. As a result, while thermal curing enhances fracture resistance initially, it may impair durability and fracture performance over time (Mi et al. [46]).

Therefore, in experimental testing of CBM's, temperature is an important factor to control during the curing process. The same material may perform weaker if it was cured for a significant amount of time with an increased temperature. This makes the thermal effects on a CBM an important mechanism to consider when possible outliers arise in experimental testing.

2.4 Summary

(1) Research does confirm that a relationship between loading rate and fracture mechanics exists. As loading rates increase on a CBM; so does the material's fracture toughness and other material properties related to fracture behavior. Research has primarily found this in mode I testing. There have also been some studies done on mode II testing – where this relationship still exists – but mode III

research is lacking. Although this is the case, there is also research that suggests the relationship between fracture behavior and loading rates is not mode dependent.

(2) There are mechanisms at play that are responsible for a CBM's sensitivity to loading rates. Many of these mechanisms make it possible for fracture behavior to improve as loading rates increase; such as inertial effects, particle interaction, and elastoviscosity. At the same time, there are also some mechanisms that could explain why the fracture behavior of the same CBM might decrease between tests – namely the materials sensitivity to thermal effects during the curing process, or the presence of pore water pressure at low loading rates. This is especially important to consider when outliers arise during experimental testing.

(3) Pore water pressure may be a key mechanism when examining a CBM's sensitivity to loading rates. At higher loading rates, the presence of pore water pressure may increase the materials properties related to fracture behavior, and at lower loading rates the pore water pressure may have the opposite effect. Pore water pressure is therefore an important mechanism to consider when any critical changes arise with fracture behavior between different levels of loading rates.

Chapter 3 Experimental Testing Program

This chapter presents the experimental testing plan developed to investigate the fracture behavior of CPB under varying curing pressures, loading rates, and curing durations. The objective of this testing program is to simulate realistic underground conditions and evaluate how these key variables influence the material's mechanical properties, with a particular focus on fracture behavior.

The experimental program involves preparing CPB samples and subjecting them to controlled curing pressures of 0 psi, 29 psi, and 58 psi. CPB has a unit weight ranging from 18-22 kN/m^3. This means that CPB curing under 10m of self weight would be curing under 200kPa (roughly 29psi), and 20m of self weight would be curing under 400kPa (roughly 58psi). Therefore, these curing pressures simulate what it would be like for CPB to cure in a mining stope, under self weight relative to those heights. To capture the effects of material aging, samples are tested at three different curing durations: 7, 28, and 90 days. These testing times allow for an overview of how the properties of the CPB may change over time as the material develops.

Following curing, the samples are tested under loading conditions corresponding to Mode I (tensile opening), Mode II (in-plane shear), and Mode III (out-of-plane shear) fracture modes. Each fracture test is conducted at displacement rates of 0.1mm/min, 1mm/min, and 10mm/min to evaluate how loading rate influences crack initiation, propagation, and overall material behavior. These displacement rates were chosen based on the literature review, where a loading rate of 1.0 mm/min was common as a standard testing rate. Examining 10mm/min and 0.1mm/min as well will then allow for the effects of different displacement rates to be analyzed. Considering all these variables, 243 tests must be performed to achieve this goal. Table 3.1 shows an overview of all the testing variables that will be changed.

Table 3.1: Testing Variables

Displacement Rate (mm/min)	Curing Time (Days)	Curing Pressure (psi)
0.1	7, 28, 90	0, 29, 58
1	7, 28, 90	0, 29, 58
10	7, 28, 90	0, 29, 58

The chapter is organized as follows: Section 3.1 describes the CPB mix design and sample preparation procedures; Section 3.2 outlines the curing process and pressure application methods; Section 3.3 provides an overview of the fracture testing setups for Mode I, II, and III; Section 3.4 explains the data analysis techniques used to calculate fracture-related properties; and Section 3.5 discusses the auxiliary analysis methods used to support interpretation of the results.

3.1 Mix Design

The cement paste backfill used in this study is prepared using a controlled mix of silica tailings, water, and Portland cement. The water-to-tailings ratio is 0.36, and the cement content is 4.5%. Cylindrical molds with a height of 20cm and a diameter of 10cm are used to hold the CPB samples as they cure. Each of these cylindrical samples can allow for three to six tests to be performed, depending on the type of testing. To reach the goal of 243 tests, 54 cylinders of CPB is needed.

An overview of the mixing procedure is as follows: first, the tailings and cement are both ‘dry-mixed’ until the materials appear to be uniform in colour. Next, the water is slowly added and thoroughly mixed over the course of about ten minutes. The CPB mix is then transferred into the previously mentioned cylindrical mold. Vibrations are then used to eliminate most air-bubbles from the cylinder of CPB. Lastly, the cylinder is then air-sealed with plastic wrap. Using the plastic wrap to seal the cylinder is a key step in the sample preparation process, since it will allow pressure to be applied to the sample as it cures. Figure 3.1 can be seen below, which gives a visual demonstration of the sample preparation procedure.

Figure 3.1: Sample Preparation Procedure Overview.

3.2 Curing Process

As previously mentioned, curing durations of 7, 28, and 90 days are utilized to investigate the fracture behavior of CPB at different stages of strengthening. To facilitate the curing process, pressure tanks were selected as a method of applying pressure to the sample throughout these durations. Pressure tanks were chosen due to their ability to cure multiple samples at the same time. Since 54 samples are needed to be cured over varying durations, pressure tanks make for a time and space efficient solution. In figure 3.2, a collection of the chosen pressure tanks can be seen:

Figure 3.2: Collection of Pressure Tanks

A keynote for the curing process is that even the samples cured under 0psi were still cured inside of the pressure tanks. This is to keep the curing environment variables, namely curing temperature, as consistent as possible.

Once the samples have been prepared, they can be placed inside of a curing tank. The tank is then filled with air until the desired level of 0psi, 29psi, or 58psi is reached. Those levels of pressure are held constant over the selected curing duration. In figure 3.3, prepared samples sitting inside of a pressure tank can be seen before they are sealed and the tank is pressurized:

Figure 3.3: Samples Inside Pressure Tank

After the curing process is complete, the samples can be prepared for each type of mode testing. The samples need to be cut into the correct dimensions, which includes cutting various notches into them. The specifics of each preparation will be discussed in section 3.3, but the procedure can be seen below in figure 3.4

Figure 3.4: Test Preparation

3.3 Testing Types

As discussed in Chapter 2, the failure of a CBM is governed by its fracture behavior. Therefore, utilizing testing that relates to fracturing is key to developing an understanding of how a CBM will respond to different loading rates and curing pressures. This study uses 3 types of tests on the prepared CPB samples, which can be referred to as Mode-I, Mode-II and Mode-II. In this section, each test will be considered in further detail.

First, Mode-I testing can be considered. Mode-I is referred to as 'opening mode'. The crack created by this type of testing has its faces move directly apart from each other. The sample is made into a semi-circle for this type of testing and has a 2.5cm notch cut into it. The semi-circle has a diameter of 10cm and a height of 5cm. The notch is cut vertically, directly in the center of the semi-circle. Figure 3.4 shows the dimensions below:

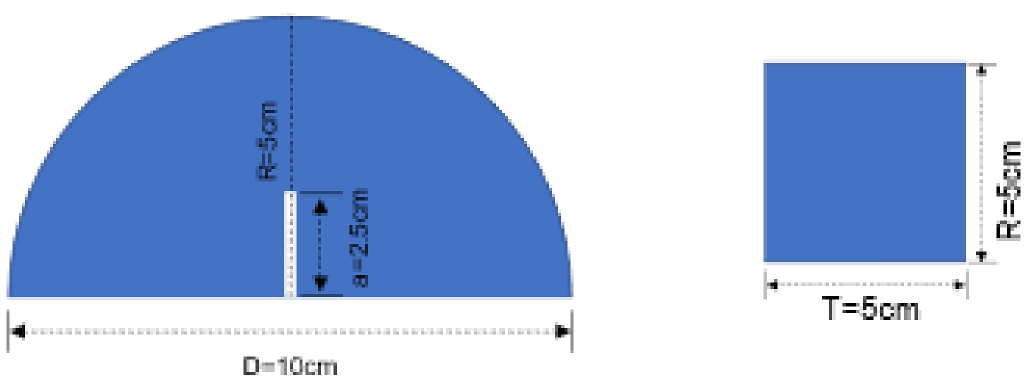

Figure 3.5: Mode 1 Sample Preparation (Cui 2023).

In mode-I testing, a compressional force is applied to induce tension. This is done by mounting the sample onto a roller support when testing with a loading frame. Figure 3.5 shows an example of a Mode I sample in its testing setup:

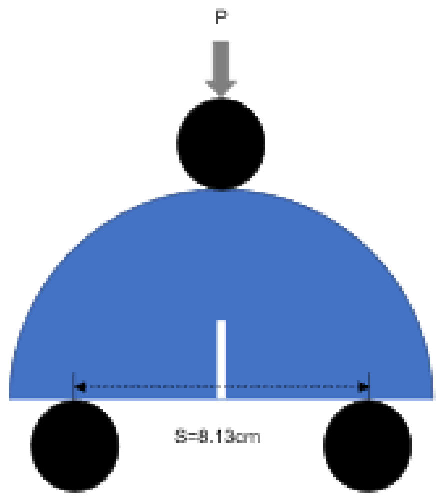

Figure 3.6: Mode 1 Test Setup (Cui 2023).

Next, Mode-II testing can be overviewed. Mode-II is referred to as ‘sliding mode’, and deals with in-plane shear forces. The crack faces created by this type of testing will slide over each other, along the plane of the crack. The sample setup for this testing is similar to mode-I, in that they are both types of semi-circular bend tests. Once again, the sample is cut into a semi-circle with a notch. The difference in sample preparation however is that the notch will be placed at an angle of 54 degrees. Figure 3.6 can be seen below as a demonstration:

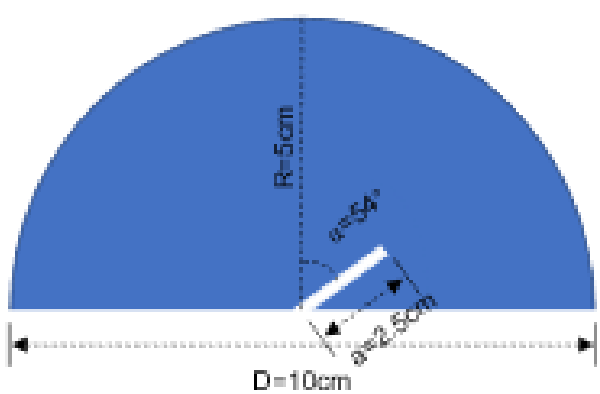

Figure 3.7: Mode 2 Sample Preparation (Cui 2023)

Mode-II testing is mounted similar to mode-I, but as mentioned, the forced being applied to the sample during the test will relate to in-plane shear. Figure 3.7 shows the Mode-II setup:

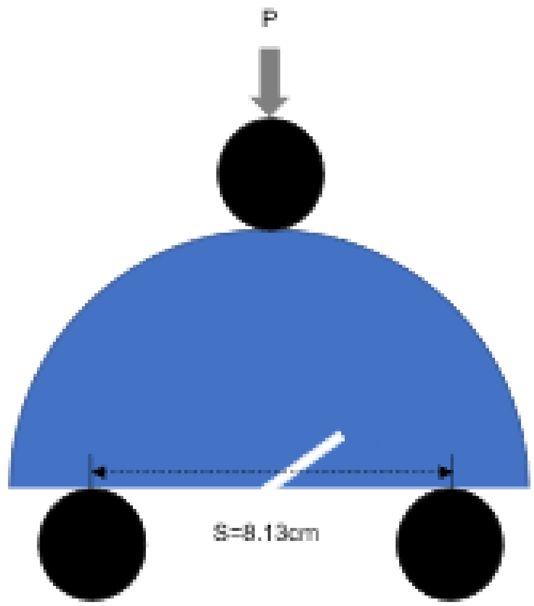

Figure 3.8: Mode 2 Test Setup (Cui 2023)

Lastly, Mode-III testing will be considered, which can be referred to as 'tearing mode.' In Mode-III testing, the crack faces are sliding against each other like mode-II testing, but this time they are sliding out-of-plane - which is related to out-of-plane shear forces. As mentioned in Chapter 2, there is a notable large gap in research relating to this type of testing. The sample preparation is a little different from the other tests in that this time an entire circular specimen is used. It still has a diameter of 10cm and a thickness of 5cm, but a 2cm notch is cut into the disk at an angle of 60% from where the force will be applied. Figure 3.8 shows how the sample will be prepared and mounted to the loading frame:

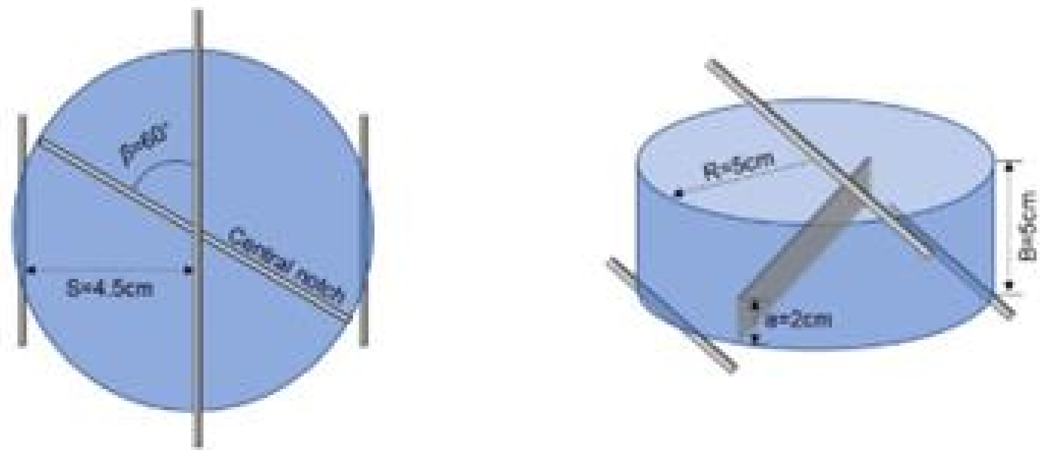

Figure 3.9: Mode 3 Sample Preparation and Test Setup (Cui 2023)

For all types of testing, a loading frame will be used to apply force to the sample. The magnitude of the force being applied increases to keep the selected displacement rate constant (for example, enough force to keep the frame moving at 1mm/min). Software will be used to keep track of the applied load over time to form a load-displacement curve, and crack propagation can be observed. From this point, data analysis can be performed.

3.4. Data Analysis

After generating load–displacement curves for all fracture tests, the resulting data is used to calculate key material properties that provide insight into the mechanical behavior of CPB. These calculated values allow for direct comparison across different displacement rates and curing pressures, helping to evaluate how these variables influence fracture performance. The primary properties examined include material stiffness, fracture toughness, energy of crack initiation, and total energy of fracture. This section outlines the methods used to calculate each parameter and discusses its relevance to better understand CPB behavior.

3.4.1 Material Stiffness

The first property to consider is material stiffness, denoted as k_i, k_{ii}, or k_{iii}, depending on the mode of testing. Material stiffness is reported in N/mm, and the calculation can be seen below in equation 1:

$$k_m = \frac{60\%F_p - 40\%F_p}{D_{60} - D_{40}} \qquad \text{Equation 1}$$

F_p, in newtons, represents the peak force recorded during testing - which typically ends up being where crack propagation begins, since the material is so brittle. The D variables are in millimetres and represent the displacement related to the associated force. For example, D_{60} would be the displacement at 60% of the peak load.

Material stiffness is a measure of how resistant a material is to deformation under applied load. In the context of CPB, stiffness provides valuable insight into the material's rigidity and its ability to provide structural support in underground mine stopes without deformation.

3.4.2 Fracture Toughness

The next property to consider is fracture toughness. Fracture toughness is calculated differently for each mode of testing but will always be reported in kPa*$m^{1/2}$. It is denoted by K_{IC}, K_{IIC}, and K_{IIIC}, depending on the mode once again. Equation 2, 3, and 4 will show how fracture toughness can be calculated for modes I, II, and III respectively:

$$K_{IC} = \frac{P}{DT}\sqrt{\pi\alpha}Y_I \qquad \text{Equation 2}$$

$$K_{IIC} = \frac{P}{DT}\sqrt{\pi\alpha}Y_{II} \qquad \text{Equation 3}$$

$$K_{IIC} = \frac{6PS}{DB^2}\sqrt{\pi\alpha}Y_{III} \quad \text{Equation 4}$$

Where:

- P = maximum peak force from the load-displacement curve (N)
- D = diameter of the specimen (m)
- T = thickness of the specimen (m)
- α = notch length (m)
- S = horizontal distance between edge bars (S = 0.045m)
- B = thickness of the specimen (m)
- Y_I¸Y_{II},$Y_{III:}$ = normalized stress intensity factor (unitless)
    - Y_I = 6.52, Y_{II} = 1.072, and Y_{III} = 0.0713

Fracture toughness quantifies a material's resistance to crack propagation. For CPB, which as mentioned is a brittle material, fracture toughness plays a critical role in determining how the material performs once cracking initiates. In the case of these tests, the crack has been initiated during sample preparation as seen in section 3.3. Fracture toughness will therefore be a key parameter in examining the sensitivity of CPB to different loading rates and curing pressures.

3.4.3 Energy of Crack Initiation

The next property to consider is the energy of crack initiation, denoted by E_c and reported in mJ. This can be found by summing the total area under the load-displacement curve for a given test, up until the peak force was reached. This can be found by using the trapezoidal rule, which approximates the area under a curve by dividing into trapezoidal sections. The area under and between two data points on the load-displacement curve can be considered a trapezoid. Its area can then be calculated, and the total area can be found by summing each section.

The energy of crack initiation represents the amount of energy a material can absorb before a crack begins to propagate. For CPB, this value is critical in assessing the material's ability to withstand deformation and stress without undergoing catastrophic failure. A higher crack initiation energy indicates a more damage-tolerant material, which is especially beneficial for maintaining stability in underground mine structures.

3.4.4 Energy of Fracture

The energy of fracture, denoted by E_f, is calculated similarly to the energy of crack initiation. It is once again the area under the load-displacement curve, but for the entire curve this time. Therefore, it can be calculated using the same method described in section 3.4.3. The only caveat is that for tests that do not see the load return to 0 after reaching the peak load, the remainder of the curve must be predicted. This is done by finding the load at the max recorded displacement during testing, and the load at 90% of that displacement. The slope between these two points can then be used to predict the remainder of the curve, until it reaches zero.

The energy of fracture reflects the total energy absorbed by the material from initial loading to complete failure, including both crack initiation and propagation. This property offers a comprehensive view of the material's toughness and its ability to dissipate energy throughout the entire fracture process. By analyzing this energy across different curing pressures and loading rates, insights can be gained into how durable and stable the material remains as complete failure begins to occur. This is something important to consider especially when it comes to safety.

3.5 Auxiliary Analysis

In addition to the data analysis of section 3.4, some different types of auxiliary analysis can be performed. These include investigating how each sample is affected by curing pressure in the following metrics: gravimetric water content, density, void ratio, degree of saturation, and microstructure.

By weighing a sample after curing, and then once again after having been dried in an oven for 24 hours, the gravimetric water content and density can be calculated. The gravimetric water content is important since it will be used to calculate the void ratio and degree of saturation. It is also a good indicator if the sealing measures used for the curing process have worked or not, since theoretically it should remain constant.

The void ratio is calculated using the volume of voids divided by the volume of solids. To find the volume of solids for a sample, the mass of solids is calculated by weighing the sample and subtracting the weight of its water - which is found using the gravimetric water content. This mass can be converted to a volume by dividing it by the specific gravity of the solids, which is estimated to be around 2.73.

Next, the volume of the voids can be found by calculating the volume of the specimen and subtracting it by the already found volume of solids. To get the volume of the specimen, the sample must be weighed again – once completely covered with paraffin wax and once submerged in water with the wax covering. The volume of the waxed specimen can be found with the principle of buoyance – taking the mass of the waxed specimen and subtracting the mass of it submerged under water. The volume of the wax itself can be found by taking the difference between the sample after and before waxing it, then and dividing it by the specific gravity of the wax (0.9). The volume of the specimen can then be found by subtracting the volume of the wax from the volume of the waxed specimen. This finally allows for calculation of the void ratio.

From there, the degree of saturation can be found by multiplying the gravimetric water content by the specific gravity of the solids (which is 2.73) and dividing that by the void ratio. In theory, higher curing pressure should lower the ratio of voids for a given sample given that there will be more compaction during curing due to pressure. This would mean, with a constant gravimetric water content, that the degree of saturation should increase with curing pressure.

4 Experimental Results

This chapter presents the results of the experimental testing program. To re-iterate what was discussed in detail during Chapter 3; load-displacement curves obtained from each test were used to calculate four key mechanical properties: fracture toughness, material stiffness, energy of crack initiation, and energy of fracture. These properties are analyzed across three different loading configurations: Mode-I (opening mode), Mode-II (sliding mode), and Mode-III (tearing mode). For each metric, results are shown for samples cured under different pressure levels (0, 29, and 58 psi) and at different curing durations (7, 28, and 90 days). Graphs are provided to illustrate trends within each mode and highlight the effects of curing pressure and loading rate on CPB performance.

An example of a typical load-displacement curve is shown in Figure 4.1 to illustrate the basis for the analysis that follows. The same type of Load-Displacement curve was created for every test performed. The solid line portion of the curve are the results directly obtained during testing. The dash line portion of the graph is the estimated portion that was discussed in chapter 3. This is done to extend the load-displacement curve until the load reaches zero, so that the energy of fracture can be calculated.

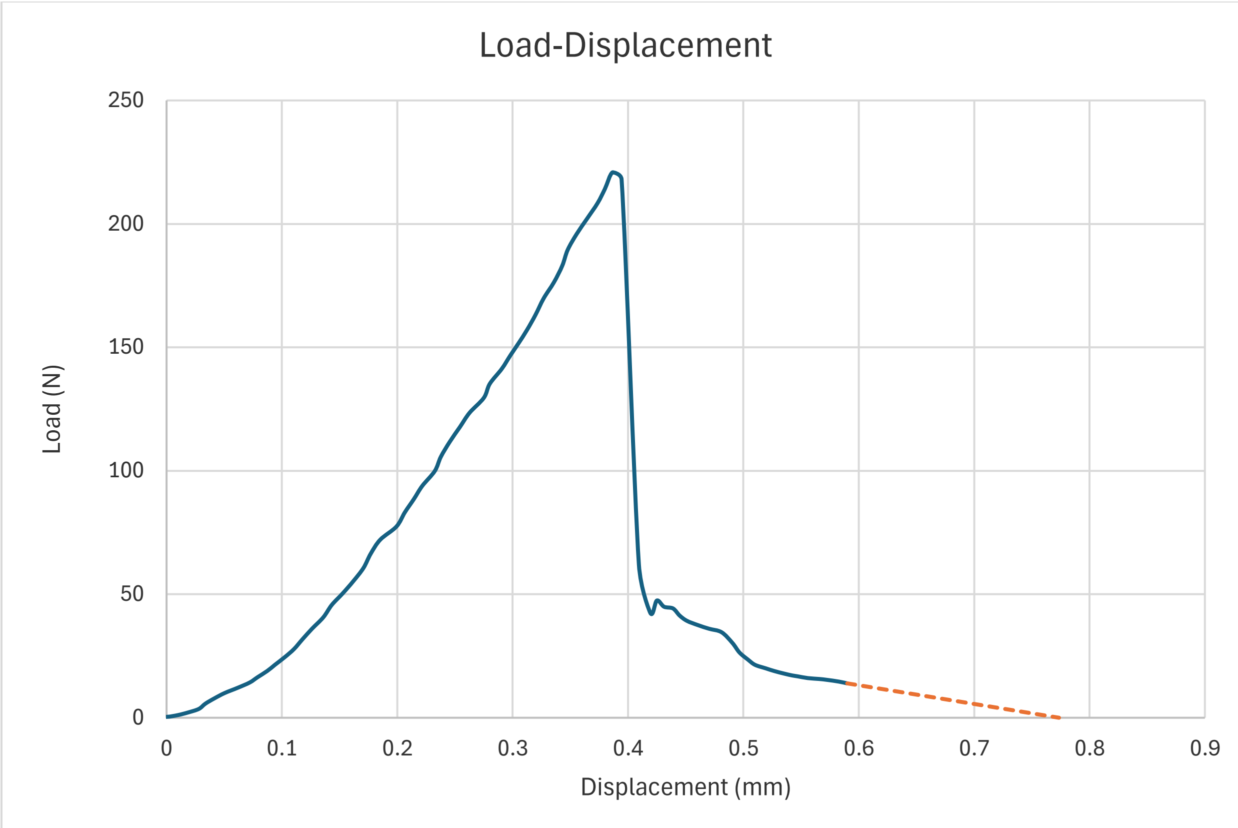

Figure 4.1: Mode 3 Load-Displacement Curve (90-days, 10mm/min, and 29psi)

4.1 Fracture Toughness

The first results to examine is the data obtained from calculating fracture toughness. To do this, three graphs have been created to visualize how loading rate, curing duration, and curing pressure affect fracture toughness. Each graph represents a different mode of testing and shows results across the three different curing durations used. Each curing duration is represented by a certain line type: short dash for 7-day, long dash for 28-day, and solid for 90-day. The data-point markers all represent a certain curing pressure: a circle for 0psi, a square for 29psi, and a triangle for 58psi.

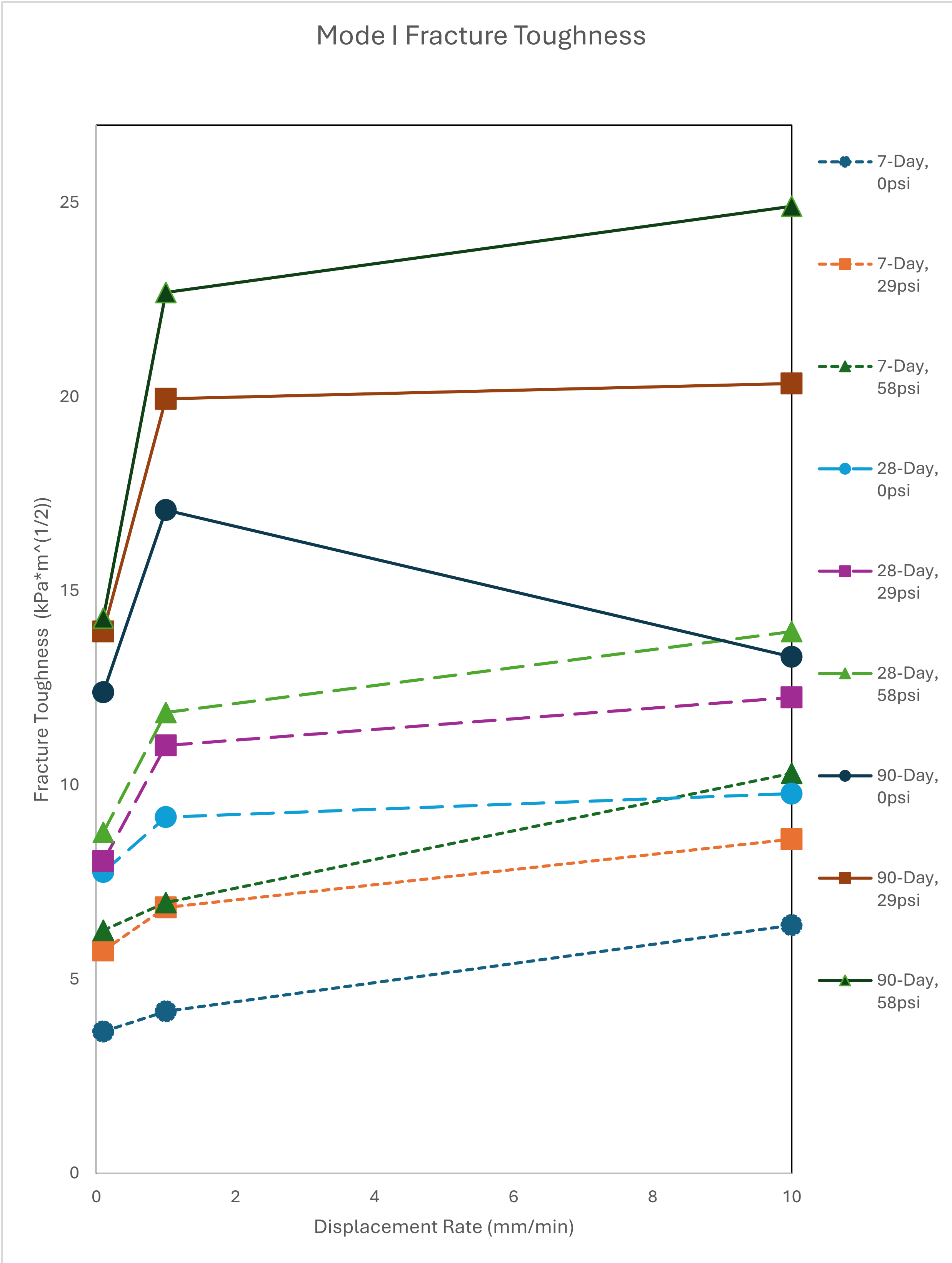

Figure 4.2: Mode-I Fracture Toughness

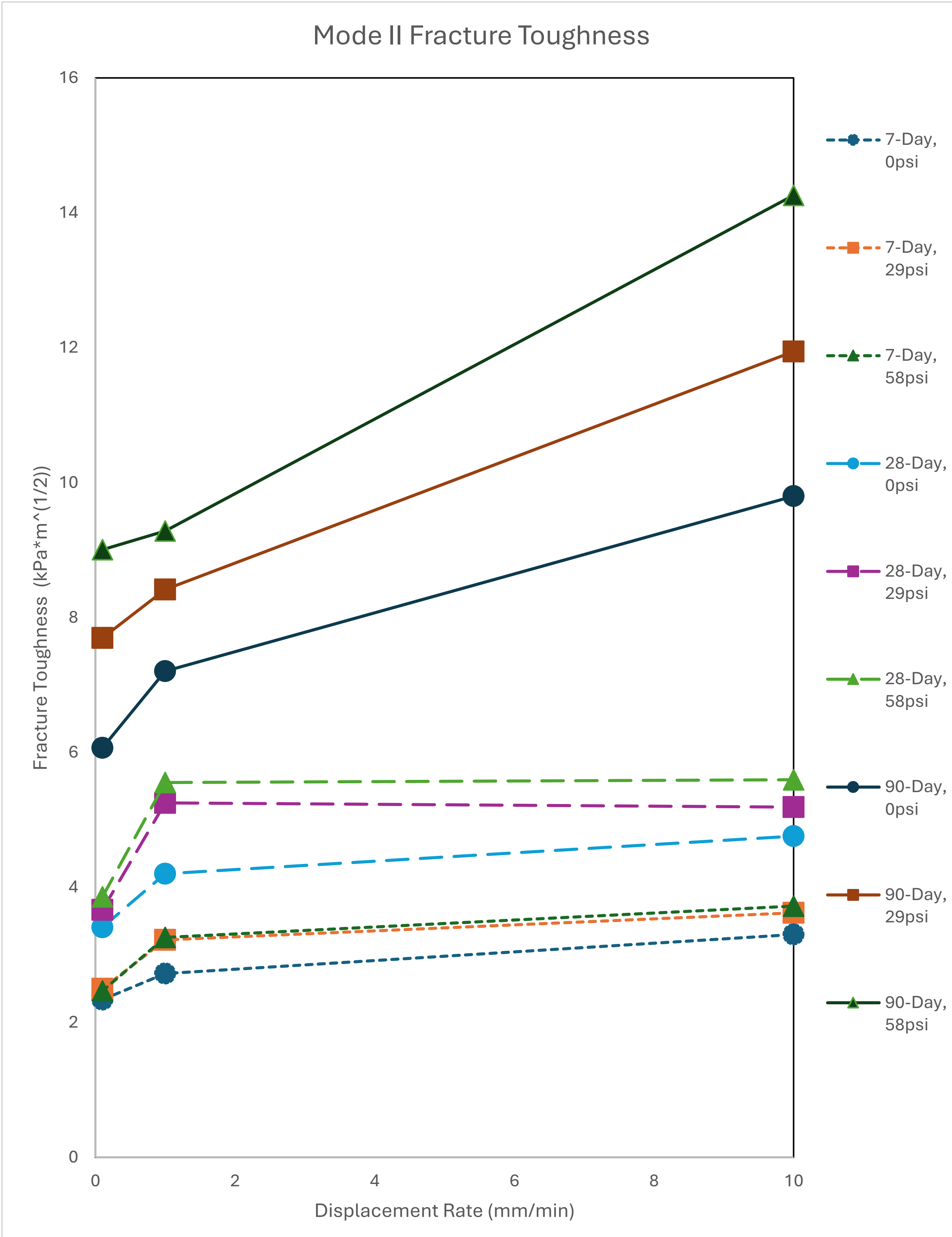

Figure 4.3: Mode-II Fracture Toughness

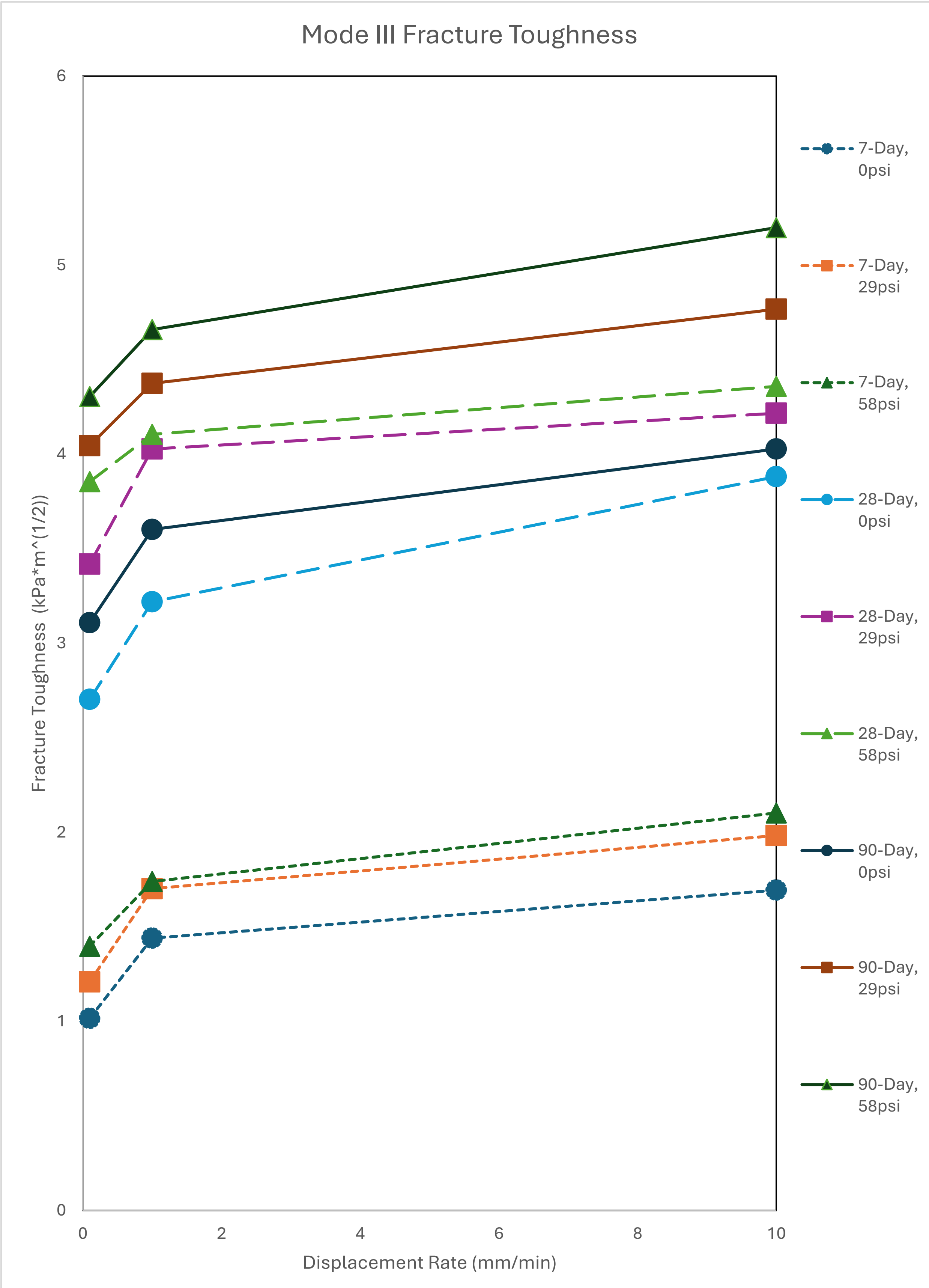

Figure 4.4: Mode-III Fracture Toughness

The first clear thing to note from graphs 4.2 to 4.4 is that curing time increases the fracture toughness of a sample under a given curing pressure for all data points. With age, CPB is clearly shown here to increase in fracture toughness as the material develops. It is known that other cementitious materials reach a large portion of their strength at 28 days but continue to strengthen as they age. After 90-days, the further increase in strength becomes very subtle. One notable trend in this study is that in mode 3 testing, the 28-day samples cured under pressure outperformed the 90-day sample cured with 0psi. This suggests that in terms of mode 3 testing, the fracture toughness increase after curing for more than 28-days is less than the fracture toughness increase gained by curing pressure.

It can also be noted that fracture toughness increases with curing pressure for a given loading rate and curing time across all testing modes. The effects of curing pressure on the structure of a CPB sample are leading to a clear increase in fracture toughness. This is less noticeable in two cases: during 7-day curing time, and during 0.1mm/min testing. For the case of 7-day curing time, this could possibly be explained by the low curing time not being enough for the effects of pressure to set in and show a noticeable change to the material. For the case of 0.1mm/min, this could possibly be due to the extra time involved that it takes for that test. The test taking place over a longer period means the material can better absorb and spread out the stress it undergoes. This implies that the theoretical effects of higher curing pressure, such as improved density and degree of saturation, do not get to show their effects on the material as well. Essentially, improved density will not matter as much if the stress is more able to distribute throughout the sample and pore water pressure is given more time to dissipate over the course of the test. These properties will be examined more in section 4.6.

The last trend to examine is how loading rate affects the fracture toughness of a sample. Overall, an increase in loading rate does result in an increase in fracture toughness across all testing modes, curing time, and curing pressure. These results confirm what was expected from the literature reviewed in Chapter 2. The mechanisms discussed in section 2.3 are clearly leading to an increase in fracture toughness with respect to loading rate. The increase from 0.1 to 1 mm/min appears to be more critical than the increase seen going from 1 to 10 mm/min. As discussed in section 2.3.4, pore water pressure could be an important mechanism to consider for explaining this critical jump. A loading rate of around 1mm/min could possibly be considered as to where the pore water pressure begins to start having its positive effects on fracture toughness. There are, however, a few outliers to the trends seen when loading rate increases. In mode-I testing, the 90-day 0psi sample shows a sharp decrease compared to the typical trend. Since this is an isolated case across that specific test, it may have been due to improper sample preparation or testing procedures. The other notable outlier to the typical trend is the 90-day mode-II testing. A possible explanation for this is that the samples tested at 1mm/min may have performed poorly; being that the outlier is seen across all 3 curing pressures. These samples were created with the same batch of CPB, which may explain where the problem comes from. The cement used to make this batch of CPB may have already been partially hydrated due to how the cement was being stored in its laboratory setting – weakening the material.

4.2 Material Stiffness

The next analysis to consider is how the material stiffness of CPB is affected by curing time, displacement rate, and curing pressure. The results of this analysis can be seen below in figures 4.5, 4.6, and 4.7, representing mode I, II, and III testing. The data is presented in the same way as the fracture toughness in section 4.1.

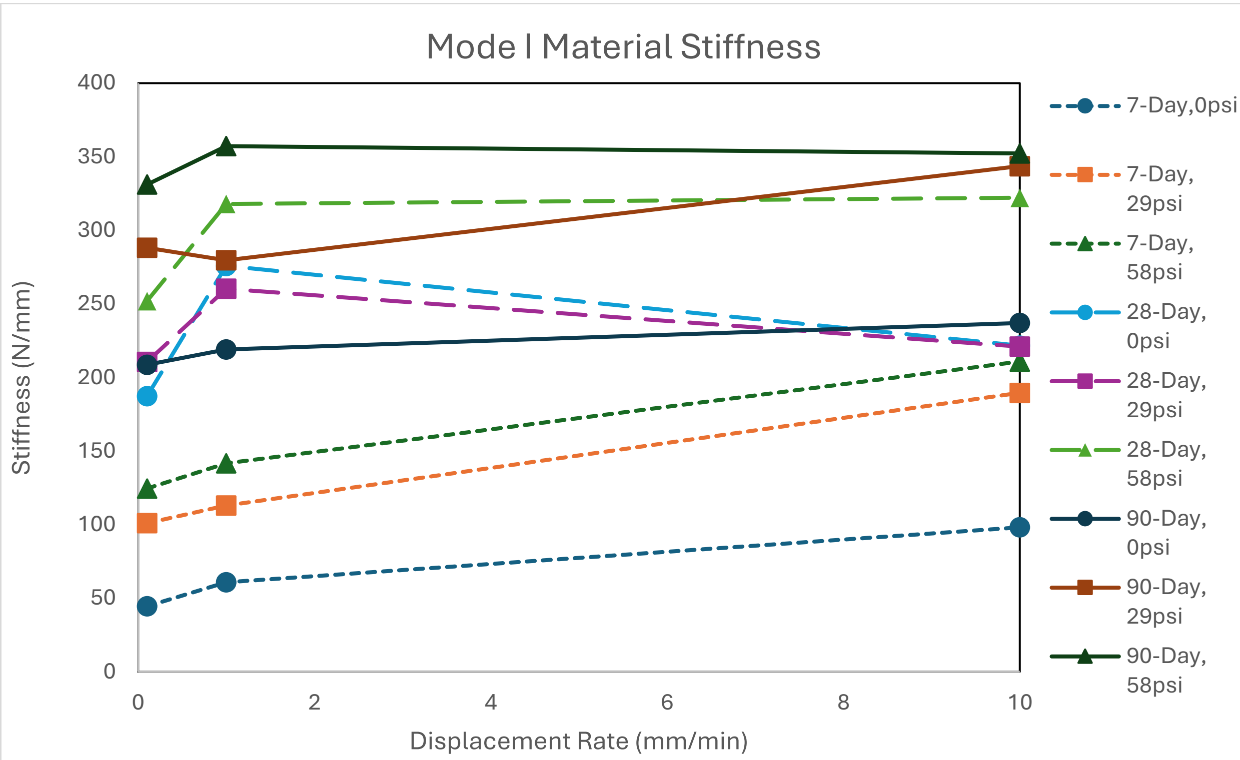

Figure 4.5: Mode I Material Stiffness

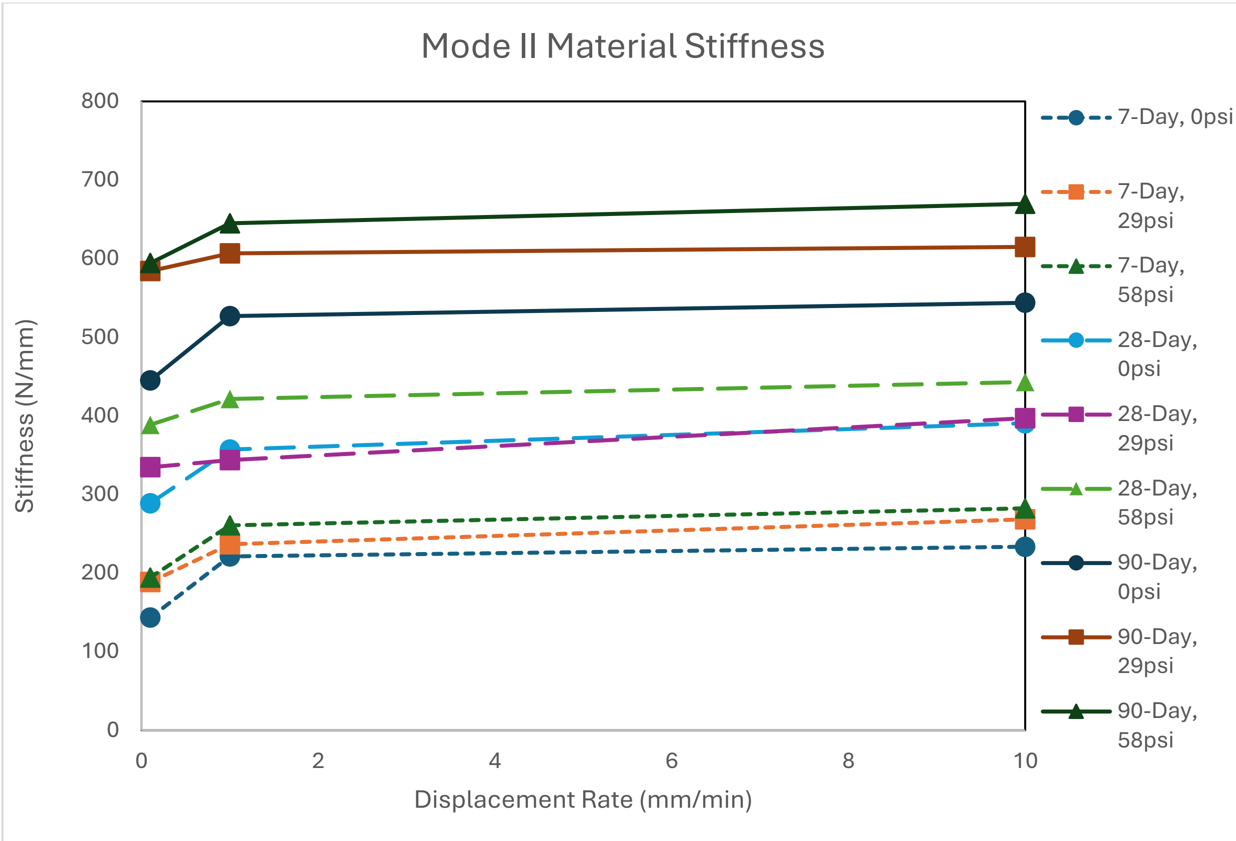

Figure 4.6: Mode II Material Stiffness

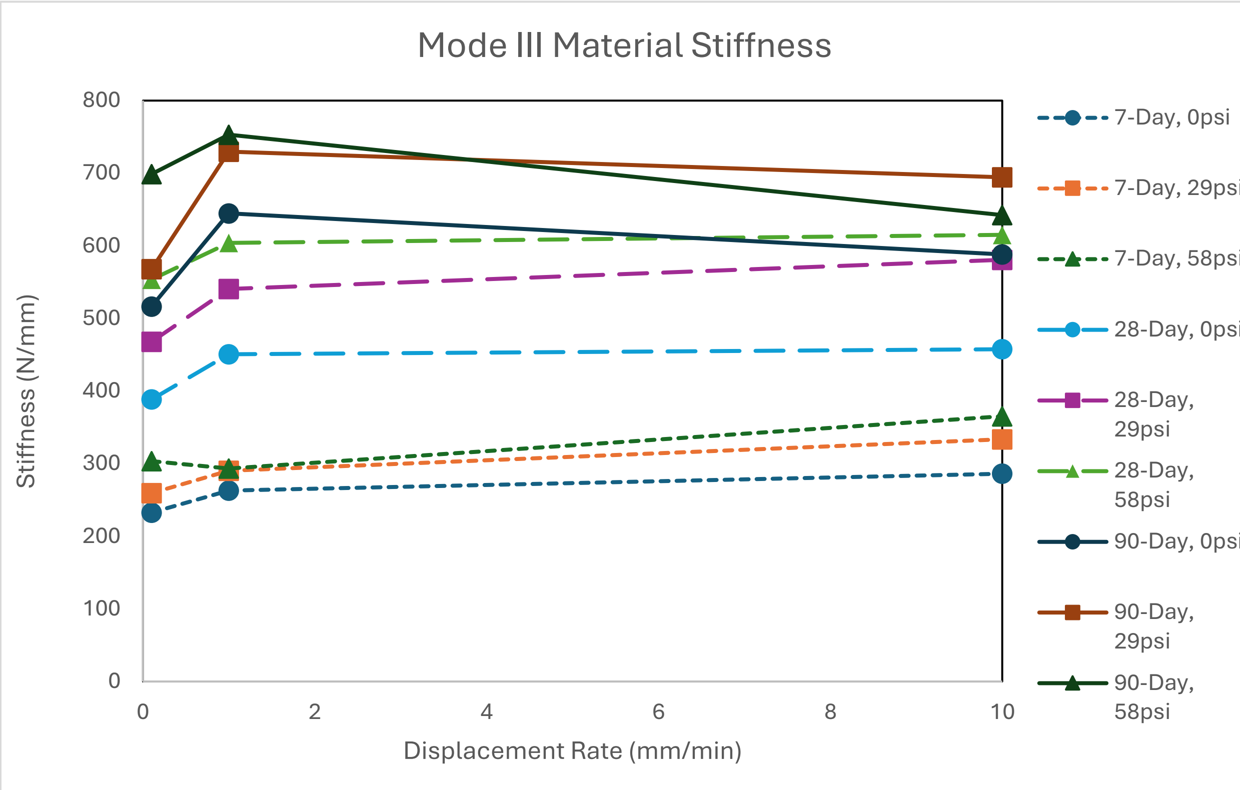

Figure 4.7: Mode III Material Stiffness

Considering the effects of curing duration again, it can be seen across all modes that there is a clear increase in material stiffness. This is comparable to other well-studied cementitious materials, such as concrete. The 7-day samples were visibly wet during handling, indicating retained moisture and an incomplete hydration reaction. Mechanically, they exhibited more ductile behavior than the 28-day and 90-day samples. This is likely due to their less developed microstructure. The 90-day samples compared to the 28-day samples still show improvement but is less noticeable, particularly in mode-I testing.

As curing pressure increases, there is a general increase in material stiffness. This increase aligns with what is expected, since a higher curing pressure should theoretically result in the CPB being more dense and less porous. Results discussed in section 4.5 can be examined to verify this as a possible explanation for the trend seen. In Mode-III testing, at 90 days and 10 mm/min, the 58psi sample was slightly less stiff than the 29psi sample. In Mode-I and II at 28 days, the 0 psi and 29 psi samples showed nearly identical stiffness values - with the 0psi sample slightly outperforming in some cases. Additionally, the 90-day 0psi sample in Mode-I at 1 mm/min displayed lower stiffness than the 28-day equivalent. These instances may perhaps be attributed to experimental variability, such as minor inconsistencies in sample preparation or microstructural factors, given that all other tests do show an increase in material stiffness with curing pressure.

The increase in displacement rate also appears to lead to a stiffer response from CPB. This again aligns with what was reviewed in chapter 2. For example: inertial effects may be adding to the apparent resistance of deformation as displacement rate increases, and at lower displacement rates the pore water pressure is given more time to migrate. Two notable outliers exist to this general trend: the mode-III 90-day samples all decrease in stiffness at 10mm/min compared to 1mm/min, as well as the mode-I 28-day 0psi and 29psi samples. The 90-day samples are theoretically the most brittle behaving samples, given their longer curing time. The higher displacement rate of 10mm/min may have caused micro-level damage before the peak load is reached, and full crack propagation occurs. This possible minor deformation may reduce stiffness. Although these samples have higher fracture toughness, this would be a possible explanation for this entire set of samples being an outlier in terms of stiffness. The 28-day 10mm/min mode-I tests as an outlier is more difficult to explain, since the 58psi test did not show the same decline in stiffness as the samples cured under lower pressure. This, coupled with the fact that this is not seen in the 7-day testing, suggests that changes occurring between 7 and 28 days influence the rate-dependent behavior. While it is true that experimental error cannot be ruled out from these results, it is possible that rate-sensitive behaviour relative to curing pressure is occurring here.

4.3 Energy of Crack Initiation

For the energy of crack initiation, the trends seen in modes 1 and 2 show some differences compared to what was seen in mode 3. To analyze these results, modes 1 and 2 can be considered first. Their data is presented similarly to the other sections once again, and can be seen below in figures 4.8 and 4.9:

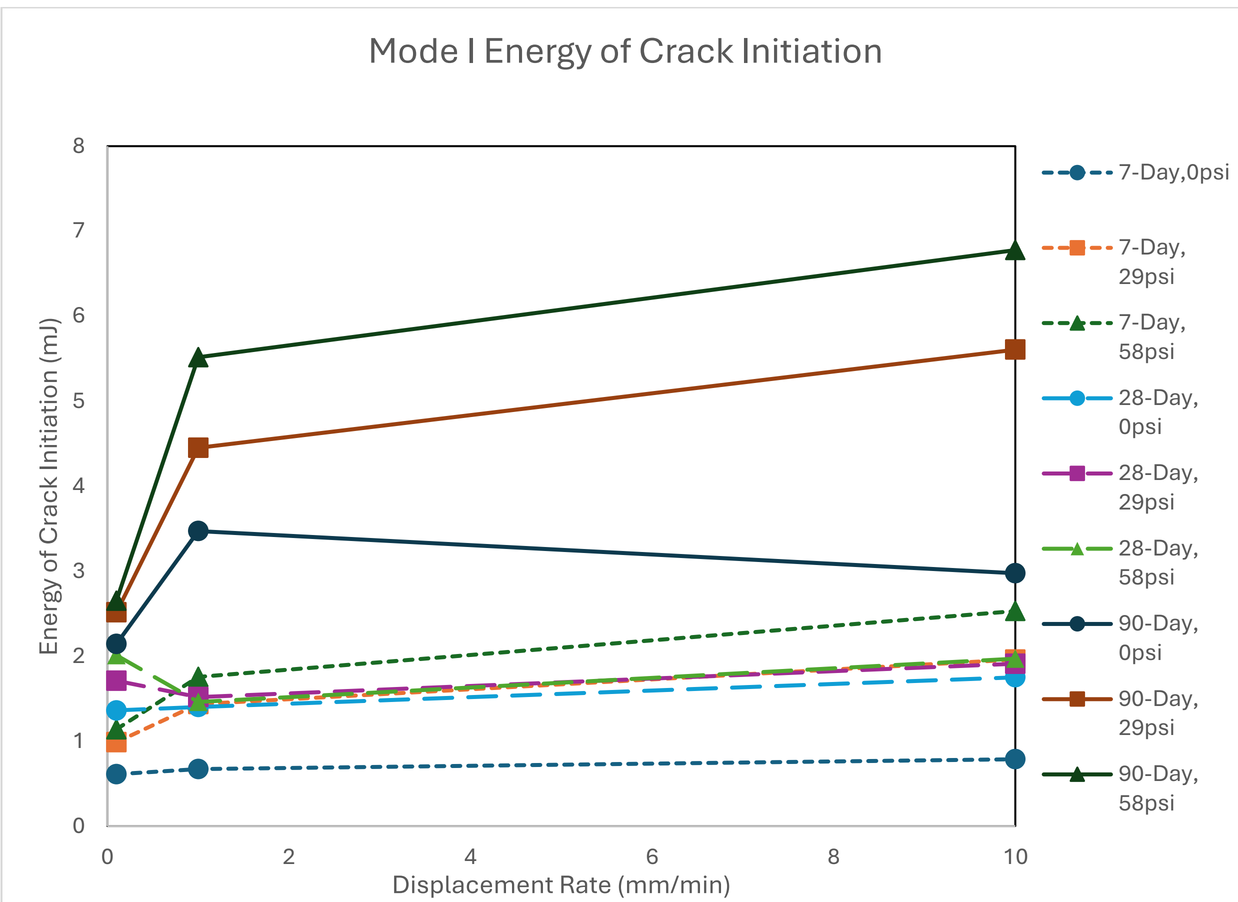

Figure 4.8: Mode-I Energy of Crack Initiation

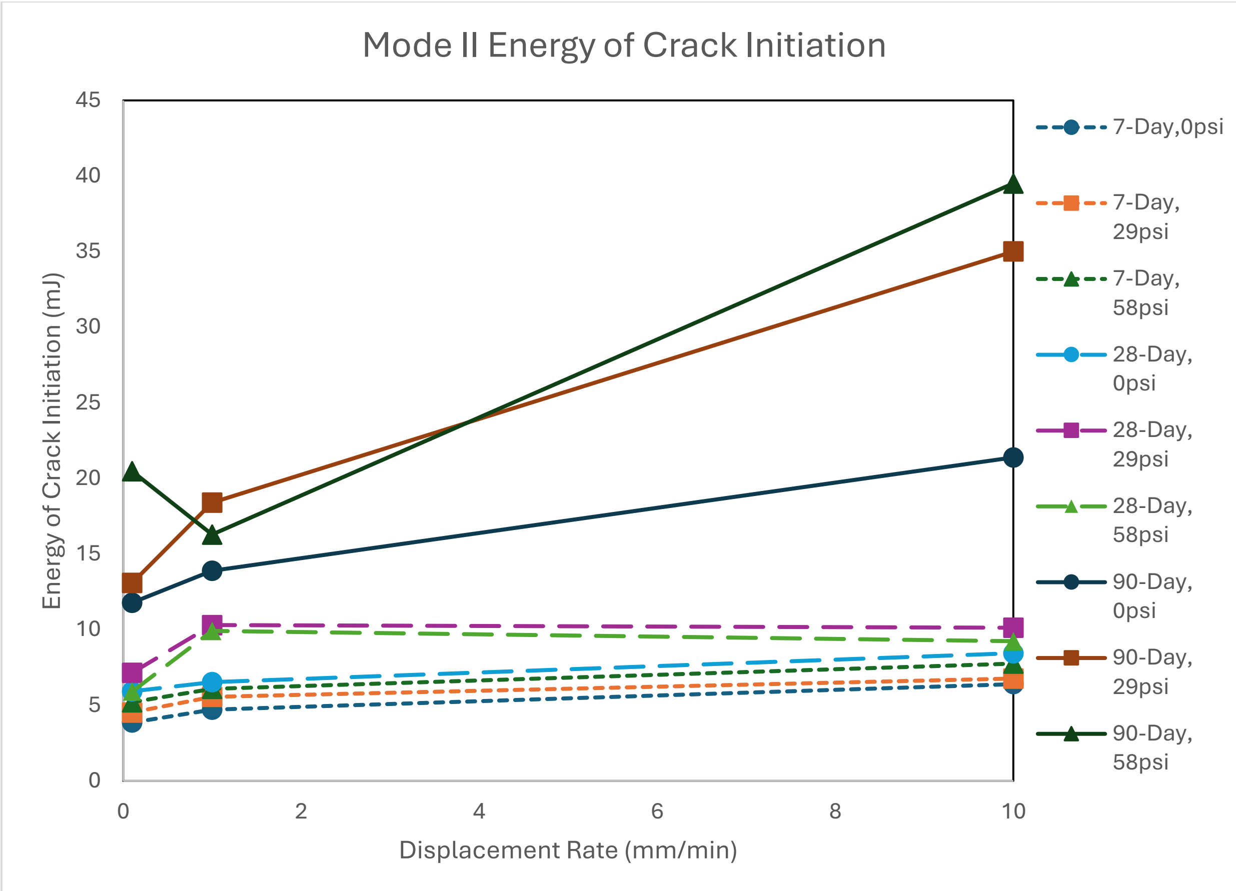

Figure 4.9: Mode-II Energy of Crack Initiation

In these modes, the energy of crack initiation does not change much between 7-day and 28-day samples. Since in most cases the 7-day samples are much lower in terms of fracture toughness and stiffness, their ductility may be giving them an advantage in this metric. The 90-day curing time is the duration that begins to show significantly more energy absorption. The effects of curing pressure are also more noticeable in the 90-day tests, where an increase in pressure does tend to result in an increase of energy of crack initiation – particularly at higher displacement rates. The differences from curing pressure seen at the lower curing times are extremely small.

Increasing displacement rate does tend to result in an overall increase in energy of crack initiation as well. The two major outliers for these trends are the 90-day mode-I sample tested at 10 mm/min, and the 90-day mode-II samples tested at 1mm/min. These outliers align with the major outliers seen examining fracture toughness, which were suspected to be due to experimental error. These results possibly reinforce that suspicion. The mode-III results are a different case however, and can be seen in Figure 4.10:

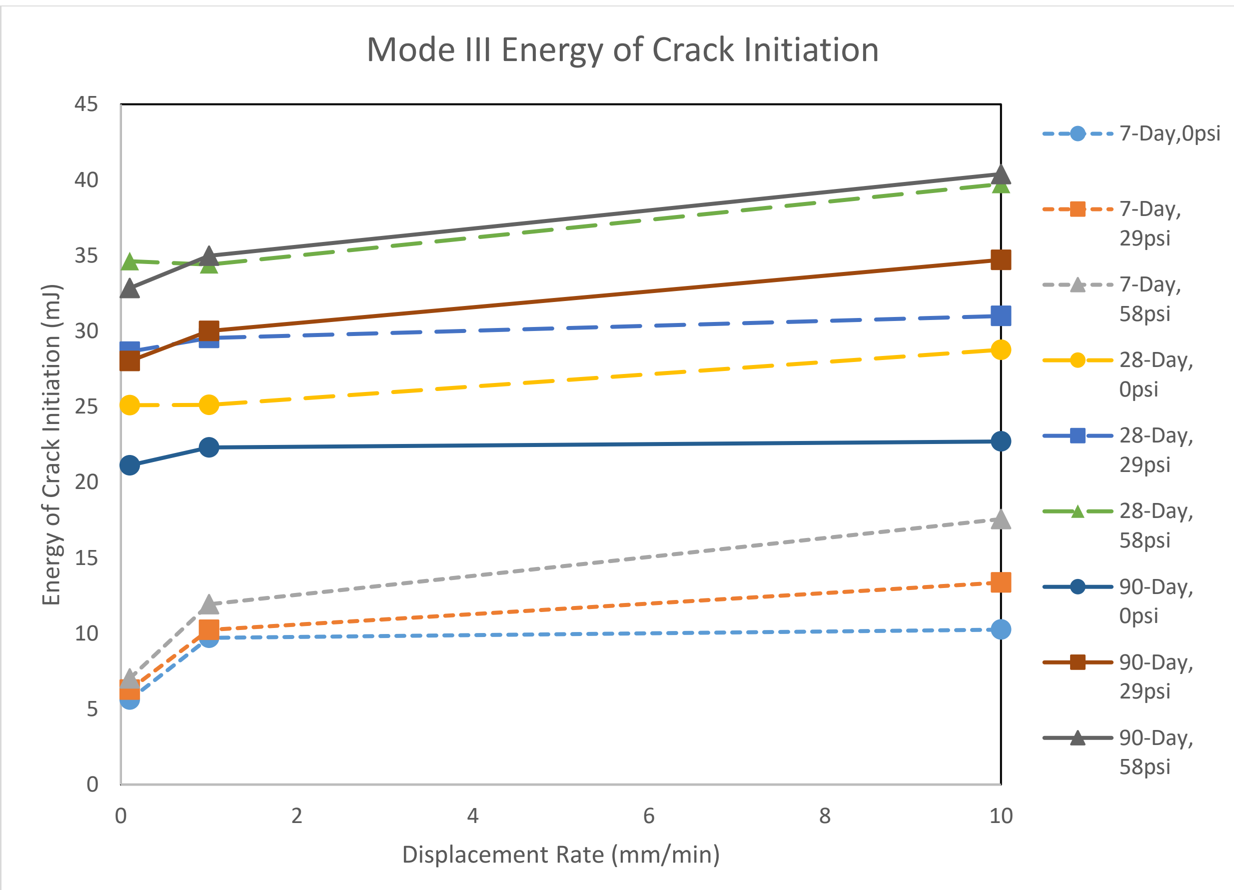

Figure 4.10: Mode-III Energy of Crack Initiation

The most significant change between mode-III and modes I and II comes from the effects of curing duration. In mode-III, the 28-day and 90-day samples perform closely, while the 7-day samples clearly absorb the least amount of energy for crack initiation. Mode-III testing does still show a clear increase in energy absorption as curing pressure was increased. The same can also be said about increasing the displacement rate.

After examining all 3 types of testing modes, there are clear mechanics at play that must be responsible for the increase in energy of crack initiation, both as curing pressure and displacement rate increase. Once again, section 4.6 will provide insight into the changes the CPB has undergone as curing pressure increase; and the mechanisms discussed in section 2.3 are possible explanations for the trends seen as displacement rate increase.

4.4 Energy of Fracture

The next metric to examine is the energy of fracture. As mentioned in chapter 3, the difference between this metric and the energy of crack initiation is that it relates to the total energy absorbed after the load-displacement curve has gone back down to zero. In almost all cases, the energy of fracture involves using a linear fit to estimate the complete load-displacement curve. Due to this, there is some uncertainty associated with the results – particularly in the lower displacement rate tests, as these typically involved more estimation. Mode-I and II can first be examined below in Figures 4.11 and 4.12, similarly to the previous section.

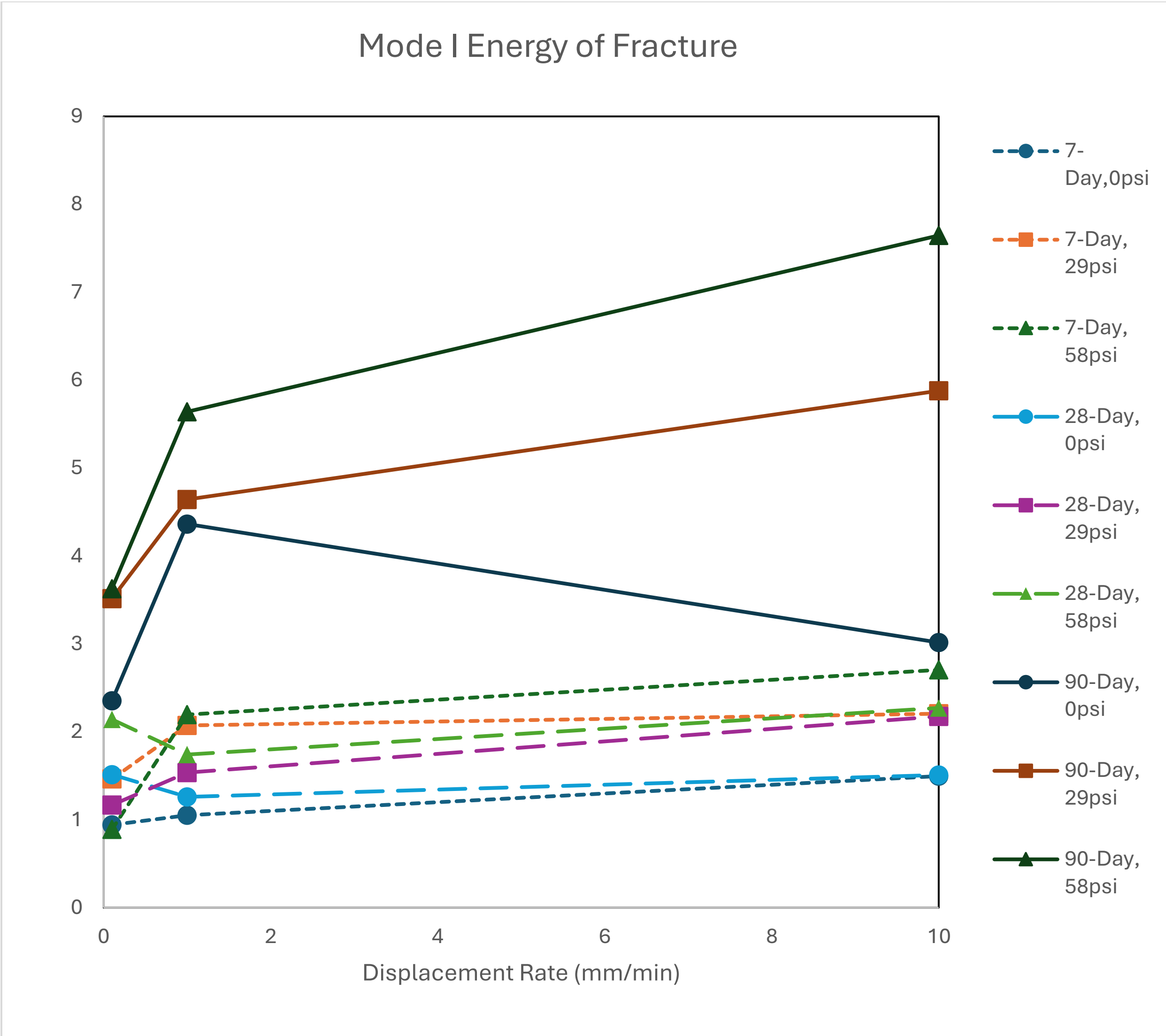

Figure 4.11: Mode-I Energy of Fracture

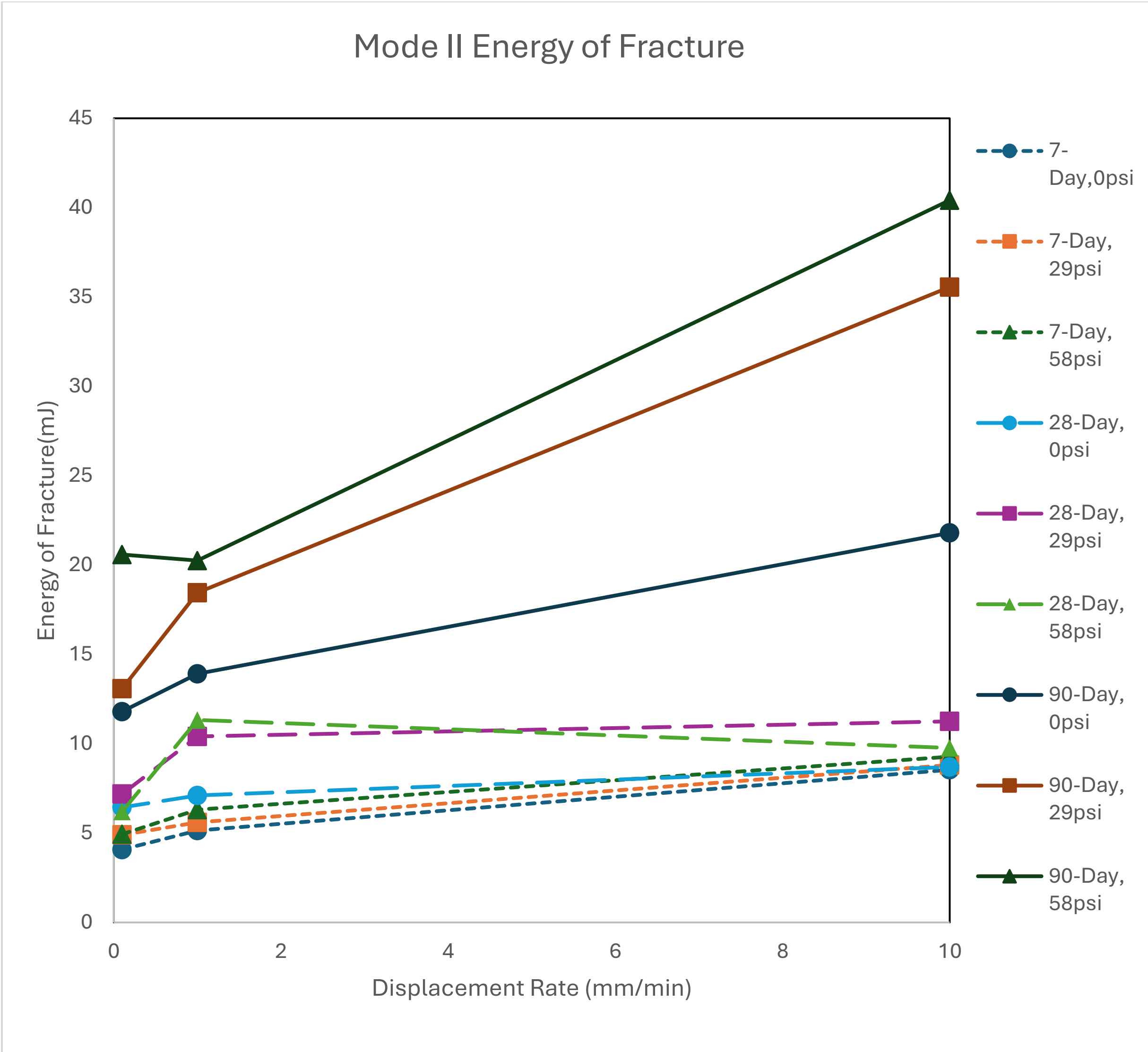

Figure 4.12: Mode II Energy of Fracture

The trends seen from modes-I and II testing are extremely close to what was seen in the energy of crack initiation, down to the outliers. The mode-III results differ more from what was seen in mode-III energy of crack initiation. They can be seen in below in figure 4.13:

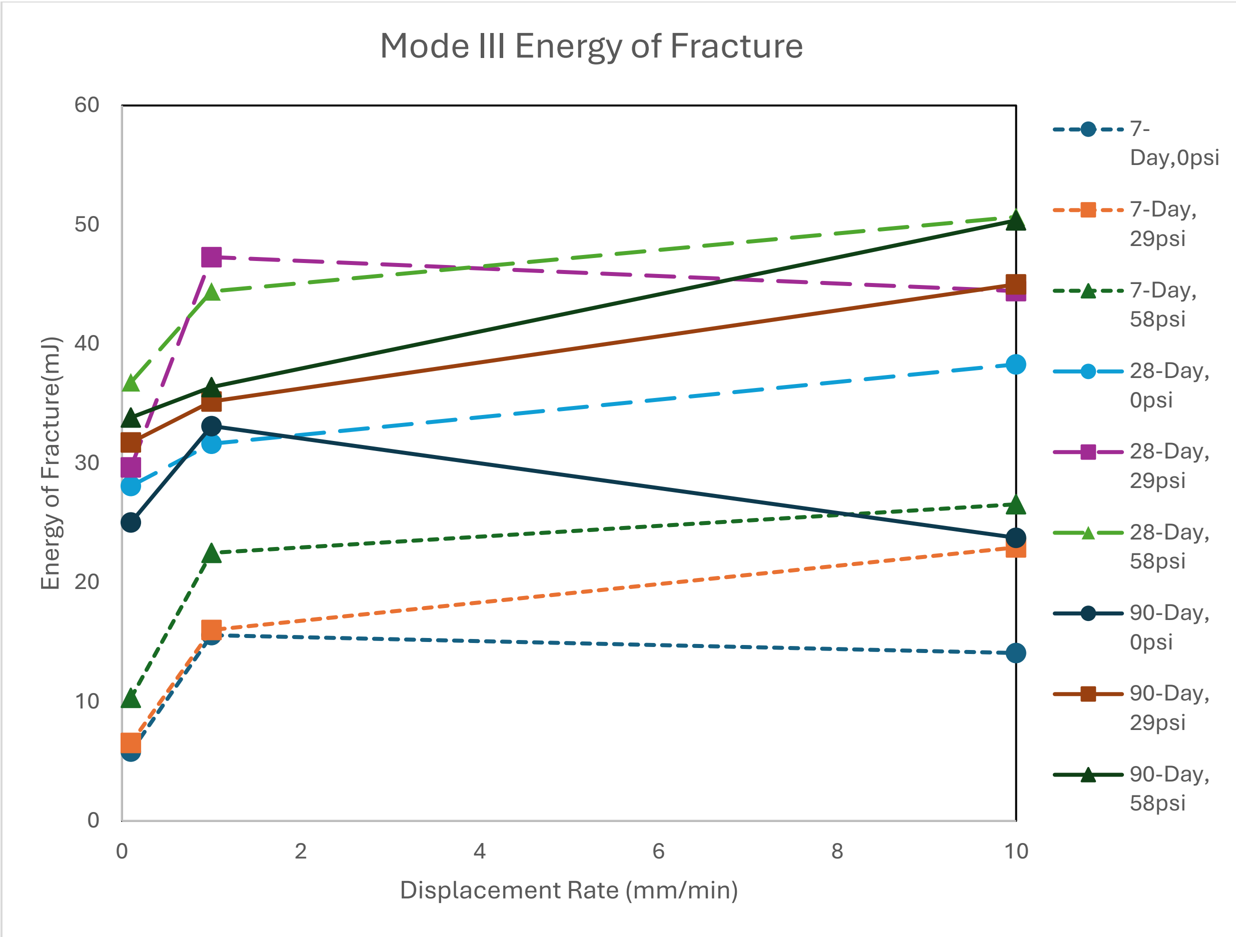

Figure 4.13: Mode-III Energy of Fracture

The mode-III results are more sporadic looking, which can perhaps be attributed to the error involved in estimating the rest of the curve. After cracking, the two halves of the mode-III samples tend to bear against each other. This causes the test to show more residual strength, which requires the load-displacement curve to involve more estimation. The 28-day samples tested at 1 mm/min especially have very rough estimates in their load-displacement curves, which helps confirm that this could be the case. In general, the difference between the energy the material absorbs when the crack is initiating compared to a complete fracture is not very high. To give a numerical example, the mode-I 28-day data can be considered by examining table 4.1 below

Table 4.1: Comparison of energy absorption for mode-I 28-day testing

Displacement Rate (mm/min)	Curing Pressure (psi)	Energy of Crack Initiation (mJ)	Energy of Fracture (mJ)	% Increase
0.1	0	5.92	6.44	8.72
0.1	29	7.15	7.19	0.55
0.1	58	5.91	6.21	5.11
1	0	6.52	7.11	8.99
1	29	10.30	10.41	1.01
1	58	9.92	11.33	14.24
10	0	8.44	8.70	3.04
10	29	10.12	11.25	11.16
10	58	9.23	9.76	5.79

The increase in the energy absorbed varies a fair amount, ranging from 0.55%, to 14.24%. As mentioned before, this is likely due to the estimation involved in calculating the energy of fracture. Despite that, the increase is notably low. Most of the energy absorption in the material occurs while the crack begins to initiate. This is due to the brittle nature of CPB. Since reaching a full fracture tends to require little additional energy, this helps confirms that the CPB's failure is governed by crack initiation. This raises the question of if CPB could benefit from some type of reinforcement, such as the inclusion of fibre in the CPB mix, to help resist crack propagation after crack initiation occurs.

4.5 Crack Propagation

In this section of the study, several figures have been included. They show CPB samples of each mode type mounted in the loading frame before they undergo testing, as well as the samples after the testing has been completed. This is to provide a visual understanding of how crack propagation occurs in each type of testing:

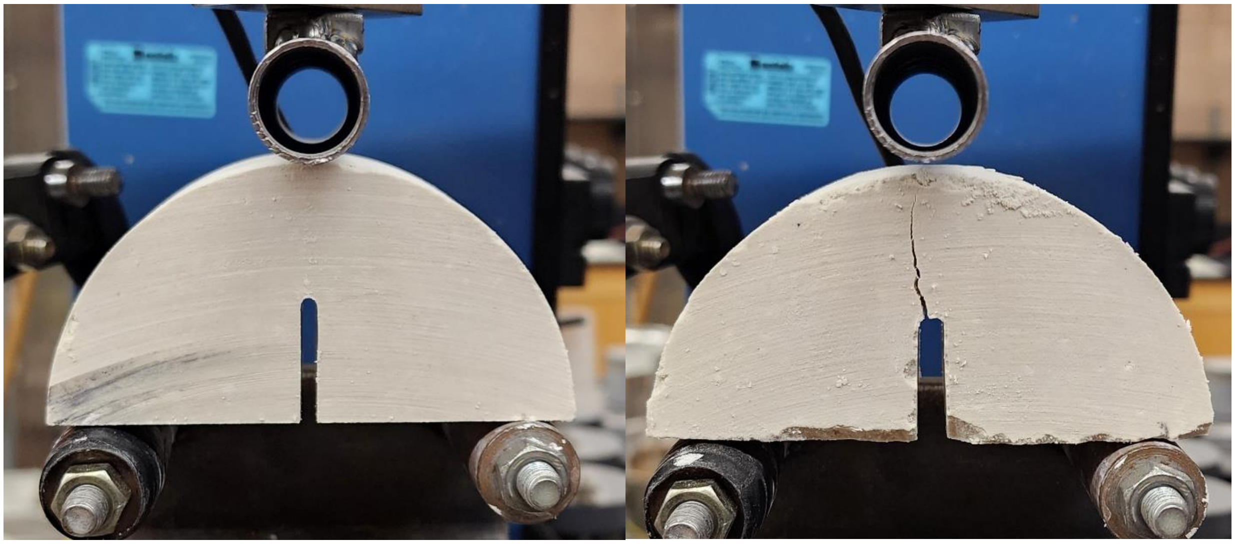

Figure 4.14: Mode-I Crack Propagation

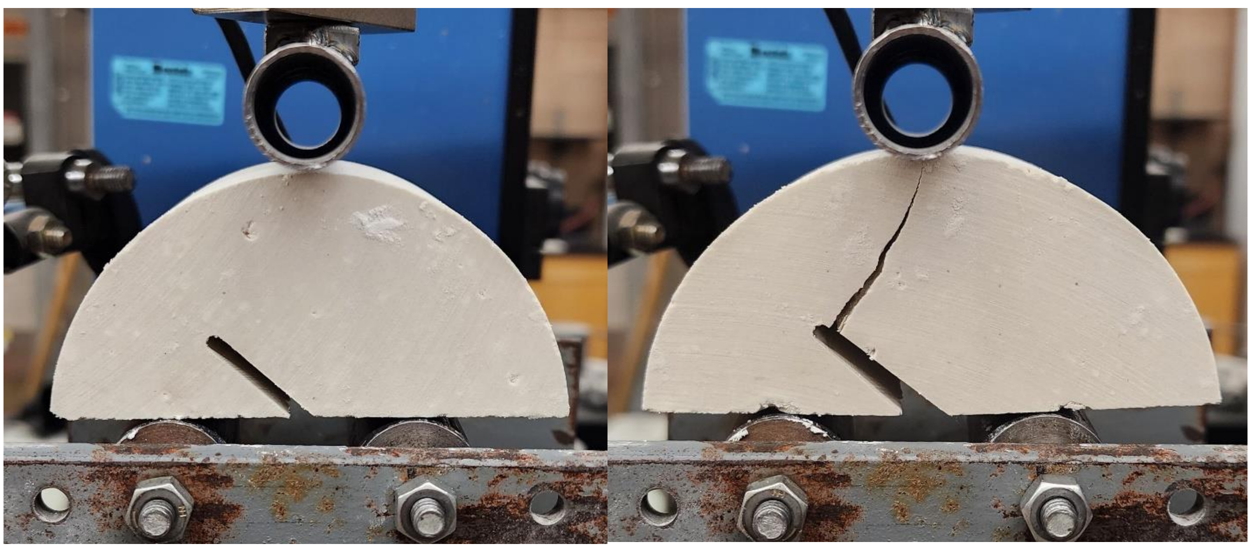

Figure 4.15: Mode-II Crack Propagation

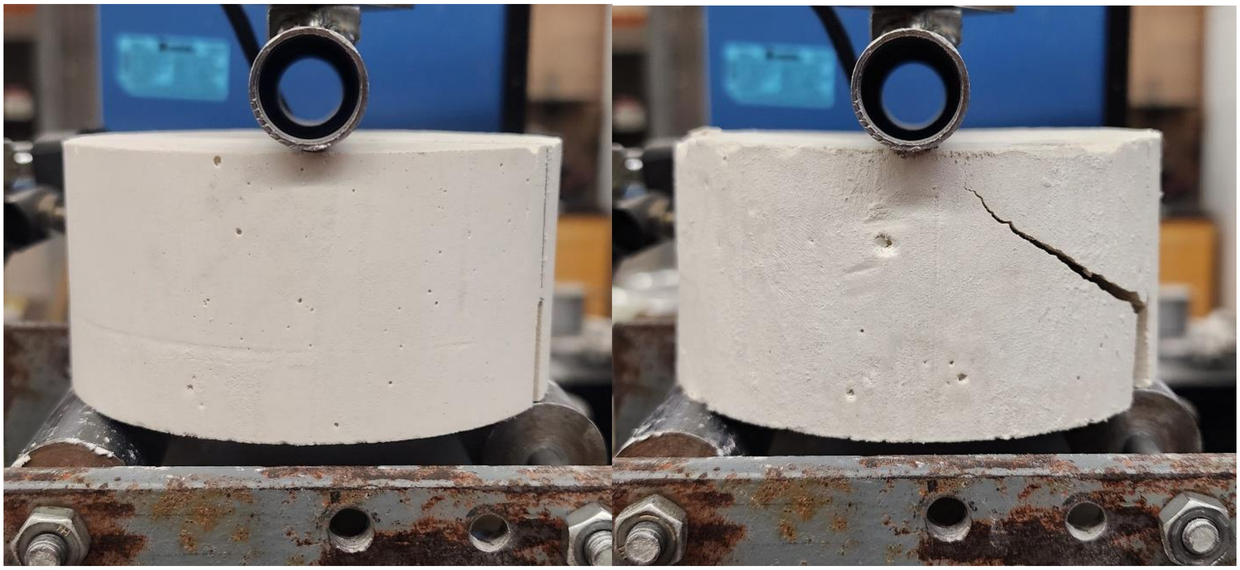

Figure 4.16: Mode-III Crack Propagation

4.6 Auxiliary Testing Results

In chapter 2, discussion was provided about what was to be expected regarding mechanical performance as displacement rate increases, and the possible mechanisms that could be causing those trends. The effects of increasing curing pressure were examined in this chapter, but not the possible mechanisms responsible for those trends. The auxiliary analysis that has been performed can now be examined to consider what mechanisms are factoring in for how CPB has improved mechanically with increased curing pressure. The results of the auxiliary analysis show the same trends and extremely similar numerical values across each curing time. The 28-day sample data can be seen below in table 4.2 to allow for consideration of the results:

Table 4.2 - 28-Day Sample Auxiliary Testing Results

Metric	Curing Pressure (psi)		
	0	29	58
Gravimetric Water Content (%)	0.32	0.32	0.32
Wet Density (g/cm^3)	1.952	1.984	1.987
Dry Density (g/cm^3)	1.479	1.496	1.499
Void Ratio (-)	0.99	0.96	0.95
Degree of Saturation (%)	0.88	0.93	0.94

The first thing to note is that the gravimetric water content has remained constant across all curing pressures. This signifies that all samples were properly sealed, and that no water was lost during the curing process. These results provide confirmation that the testing setup – particularly how the samples were sealed inside the cylinders – functioned as intended.

The wet and dry densities of samples improved as curing pressure increased. An increase in density relating to an increase in curing pressure is a clear possible mechanism that explains the trends seen in the mechanical performance of CPB. It can also be noted that the difference between 0psi and 29psi is more significant than the difference between 29psi and 58psi, which imply that the effects of pressure on density will eventually plateau.

Void ratio and degree of saturation also see changes relative to curing pressure. As curing pressure increases, there are slightly less voids present in the sample. Simultaneously, as less voids become present and compaction occurs, the degree of saturation is improved. The change in the microstructure relating to void ratio could have potential effects on the mechanical performance of the CPB, although the change is very minimal. This signifies that the void ratio is not overly sensitive to the effects of curing pressure. The changes seen in the degree of saturation are also small, however, this increase does mean that there will be a larger presence of pore water pressure. Pore water pressure has already been discussed in chapter 2 about its effects on a CBM relating to displacement rate. Since a higher curing pressure leads to a higher degree of saturation, the degree of saturation is an important mechanism to consider when noting that the effects of curing pressure are more pronounced at higher displacement rates.

5 Conclusions and Recommendations

5.1 Conclusions

This study examined the fracture behavior of cemented paste backfill (CPB) under varying curing times, curing pressures, and displacement rates, across Mode I (tensile opening), Mode II (in-plane shear), and Mode III (out-of-plane shear) fracture modes. The findings provide new insight into how these key variables influence fracture toughness, stiffness, and energy absorption, offering a more realistic understanding of CPB performance under underground mining conditions.

Fracture toughness consistently increased with curing time, curing pressure, and displacement rate. The largest gains occurred between 7- and 28-day curing, with toughness often more than doubling in this period across all modes, while improvements from 28 to 90 days were smaller. Curing pressure played a particularly strong role: for example, in Mode III testing, a 28-day sample cured at 29 psi outperformed a 90-day sample cured at 0 psi, underscoring the significance of curing under realistic field confinement. Displacement rate also strongly affected toughness, with the increase from 0.1 to 1 mm/min being more critical than the change from 1 to 10 mm/min. This suggests a pore water pressure effect, where faster loading reduces drainage and temporarily strengthens the material. Across modes, Mode I and II displayed similar sensitivity to these variables, while Mode III consistently produced higher absolute toughness values, reflecting its resistance to out-of-plane shear fracture.

Material stiffness followed similar trends, improving with curing time, curing pressure, and displacement rate. Seven-day samples were visibly weaker and more ductile, whereas 28- and 90-day samples developed much stiffer responses, aligning with their more mature hydration and microstructure. For example, stiffness values in Mode I nearly doubled between 7 and 28 days. Higher curing pressure generally produced denser, stiffer specimens, though some variability was observed, particularly at 28 days where 0 psi and 29 psi samples were comparable. Displacement rate effects were also evident, with stiffness increasing at faster rates due to inertial and elastoviscous mechanisms, although Mode III 90-day samples displayed a notable decline at 10 mm/min, suggesting brittle micro-damage at high loading speeds.

Energy of crack initiation was more sensitive to curing time than toughness or stiffness. Seven- and 28-day samples showed comparable energy absorption, but 90-day samples consistently absorbed far more energy before crack initiation, particularly in Modes I and II. For instance, Mode I energy of crack initiation increased nearly threefold between 28 and 90 days at higher curing pressures. Curing pressure effects were again most pronounced at 90 days, where denser structure and higher saturation improved resistance to fracture. In Mode III, however, 28- and 90-day samples behaved similarly, suggesting that out-of-plane shear cracks are less sensitive to long-term curing than tensile or in-plane shear cracks. Increasing displacement rate also enhanced crack initiation energy across all modes, reinforcing the role of pore water pressure and particle interaction in delaying fracture.

Total fracture energy showed trends consistent with crack initiation energy, although the reliance on estimated post-peak curves introduced some variability, especially at low displacement rates. Despite this uncertainty, fracture energy generally increased with curing time, curing pressure, and loading rate. The difference between initiation and total fracture energy was relatively small, confirming that most of the energy in CPB fracture is consumed at crack initiation rather than propagation. Mode III tests exhibited more scatter due to residual bearing after fracture but still demonstrated higher absolute fracture energies than Modes I and II.

Overall, the results confirm that CPB mechanical performance is highly dependent on curing time, curing pressure, and displacement rate. Curing pressure produced improvements comparable to or greater than long-term curing, emphasizing the importance of testing CPB under confined conditions that reflect in-situ environments. Displacement rate effects highlight the need to look beyond standard testing rates, as results at 0.1 mm/min and 1 mm/min diverged significantly. Across fracture modes, Mode III generally produced the highest toughness and energy values, while Mode I and II showed more pronounced sensitivity to curing and rate effects. These findings contribute to a better understanding of CPB's fracture behavior and provide guidance for safer and more reliable mine backfill design and testing practices.

5.2 Recommendations

These conclusions are based on the overall trends seen in the results. However, a few outliers have been pointed out in chapter 4. It is recommended that the testing be repeated for 90-day mode-II samples under all curing pressures at 1 mm/min, and the 90-day mode-I sample under 0psi at 10 mm/min. The results for those tests are the more noticeable outliers seen, and it would be beneficial to better understand the mechanical performance of CPB at those testing parameters. Aside from that, further testing to explore both higher and lower displacement rates could also be beneficial. It is expected that both further increasing and decreasing the displacement rate may show that the mechanical performance begins to plateau at a certain level. This would further highlight the existence of a ‘critical’ loading rate in terms of a better mechanical behavior of CPB. The same could also be said about experimenting on higher levels of curing pressure.

References

[1] Xinxin Nie, Qian Yin, Qi Wang, Minghui Ren, Tianci Deng, Hongwen Jing, Qiang Zhang, Jiangyu Wu, "Investigating mechanical properties of cemented gangue backfill materials subjected to static-dynamic combined loads." Construction and Building Materials, Volume 400, 2023.

[2] Weiwei Lin, Teruhiko Yoda, "Chapter Four - Loads and Load Distribution." Bridge Engineering, Butterworth-Heinemann, 2017.

[3] Shigeru Shimizu, "Behaviour of steel columns under 3-D seismic load." Thin-Walled Structures, Volume 49, Issue 5, 2011.

[4] Brady & Brown, "Rock Mechanics for Underground Mining." 2006

[5] Singh & Goel, "Blast-induced ground vibrations in mines." 2006.

[6] Mark & Kruege, "Mining Equipment Loadings on Rock." 2015

[7] Davis et al., "Equipment impact loads in underground mining." 2013

[8] Hudson & Harrison, "Engineering Rock Mechanics." 1997

[9] Hagan & Williams, "Ground Support Loading Rates." 2010

[10] X.X. Zhang, G. Ruiz, R.C. Yu, M. Tarifa, "Fracture behaviour of high-strength concrete at a wide range of loading rates." International Journal of Impact Engineering, Volume 36, Issues 10–11, 2009

[11] Weina Meng, Yiming Yao, Barzin Mobasher, Kamal Henri Khayat, "Effects of loading rate and notch-to-depth ratio of notched beams on flexural performance of ultra-high-performance concrete." Cement and Concrete Composites, Volume 83, 2017.

[12] Neville, "Properties of Concrete." 1995.

[13] Lok & Pei, "Dynamic behavior of concrete in compression." 1998.

[14] Ross et al., "Effects of strain rate on concrete strength." 1995

[15] Malvar & Ross, "Review of strain rate effects for concrete in tension." 1998

[16] Reinhardt et al., “Fracture mechanics of concrete under dynamic loading.” 1986

[17] Wittmann, “Fracture energy of concrete.” 1983

[18] Consoli et al., “Key parameters for strength control of artificially cemented soils.” 2007

[19] Consoli et al., “Strength behavior of compacted soil-fly ash mixtures.” 2009

[20] Assaad et al., “Stabilization of fine-grained soils using cementitious materials.” 2007.

[21] Shin et al., “Flexural behavior of cement-treated soils.” 2002.

[22] Yu et al., “Fracture characteristics of cemented soils.” 2018.

[23] Fall et al., “Coupled thermohydro-mechanical modeling of cemented paste backfill.” 2010.

[24] Yilmaz et al., “Strength development of CPB with different binders.” 2014.

[25] Belem et al., “Characterization of tensile strength in cemented paste backfill.” 2002.

[26] Li & Fall, Fracture energy of cemented paste backfill at early ages.” 2016.

[27] Hongjian Lu, Chongchong Qi, Qiusong Chen, Deqing Gan, Zhenlin Xue, Yajun Hu, “A new procedure for recycling waste tailings as cemented paste backfill to underground stopes and open pits.” Journal of Cleaner Production, Volume 188, 2018.

[28] D. Marchon, R.J. Flatt, “8 - Mechanisms of cement hydration.” Science and Technology of Concrete Admixtures, Woodhead Publishing, 2016.

[29] M.R. Ayatollahi, M.R.M. Aliha, “On the use of Brazilian disc specimen for calculating mixed mode I–II fracture toughness of rock materials.” Engineering Fracture Mechanics, Volume 75, Issue 16, 2008.

[30] Liang Cui, Aaron McAdie. “Experimental study on evolutive fracture behavior and properties of sulfate-rich fiber-reinforced cemented paste backfill under pure mode-I, mode-II, and mode-III loadings,” 2023.

[31] Shunchuan Wu, Wei Sun, Xueliang Xu, “Study on mode I fracture toughness of rocks using flat-joint model and moment tensor.” Theoretical and Applied Fracture Mechanics, Volume 120, 2022.

[32] Kuruppu, M.D., Obara, Y., Ayatollahi, M.R. *et al.* ISRM-Suggested Method for Determining the Mode I Static Fracture Toughness Using Semi-Circular Bend Specimen. *Rock Mech Rock Eng* 47, 267–274 (2014).

[33] Soo-Ho Chang, Chung-In Lee, Seokwon Jeon, "Measurement of rock fracture toughness under modes I and II and mixed-mode conditions by using disc-type specimens." Engineering Geology, Volume 66, Issues 1–2, 2002.

[34] Zhanguo Xiu, Shuhong Wang, Yingchun Ji, Feili Wang, Fengyu Ren, Van-Tuan Nguyen,"Loading rate effect on the uniaxial compressive strength (UCS) behavior of cemented paste backfill (CPB)." Construction and Building Materials, Volume 271, 2021.

[35] Xuepeng Song, Junbiao Li, Shi Wang, Shuang Zhou, Wu Liu, Yuankai Zhai, Yuxin Hao. "A Study of mechanical behavior and cracking mechanism of prefabricated fracture cemented paste backfill under different loading rates from the perspective of energy evolution." 2022.

[36] Min-Hua Ma, Zhi-Min Wu, Jian-Jun Zheng, Yan-Jie Wang, Rena C. Yu, Xiao-Dong Fei, "Effect of loading rate on mixed mode I-II crack propagation in concrete." Theoretical and Applied Fracture Mechanics, Volume 112, 2021.

[37] Saadati Y, Chatelain J-F, Lebrun G, Beauchamp Y, Bocher P, Vanderesse N, "A Study of the Interlaminar Fracture Toughness of Unidirectional Flax/Epoxy Composites." *Journal of Composites Science*. 2020; 4(2):66.

[38] Kun Fang, Lei Ren, Haiqiang Jiang, "Development of Mode I and Mode II fracture toughness of cemented paste backfill: Experimental results of the effect of mix proportion, temperature and chemistry of the pore water." Engineering Fracture Mechanics, Volume 258, 2021.

[39] Fang, K., Cui, L. "Experimental investigation of evolutive mode-I and mode-II fracture behavior of fiber-reinforced cemented paste backfill: Effect of curing temperature and curing time." *Front. Struct. Civ. Eng.* 17, 256–270, 2023.

[60] Shuling Gao, Rongrong Gao, Ru Mu, Yanping Zhu, Lin Qi, “Effect of loading rate on mode I/mode II/mixed mode I–II fracture performance of engineered cementitious composites.” International Journal of Solids and Structures, Volumes 262–263, 2023.

[41] Nitka, M., Tejchman, J, “Effects of aggregate crushing and strain rate on fracture in compressive concrete with a DEM-based breakage model. *Granular Matter* 27, 8 2025.

[42] Jianzhong Lai, Wei Sun, “Dynamic behaviour and visco-elastic damage model of ultra-high performance cementitious composite.” Cement and Concrete Research, Volume 39, Issue 11, 2009, Pages 1044-1051.

[43] Zhang P, Wu Z, Liu Y, Chu Z, “Numerical Study on the Dynamic Fracture Energy of Concrete Based on a Rate-Dependent Cohesive Model.” *Materials*. 2021; 14(23):7421.

[44] Shilko EV, Konovalenko IS, Konovalenko IS, “Nonlinear Mechanical Effect of Free Water on the Dynamic Compressive Strength and Fracture of High-Strength Concrete.” Materials (Basel). 2021 Jul 18

[45] Bažant, Z.P., Najjar, L.J, “Nonlinear water diffusion in nonsaturated concrete.” *Mat. Constr.* 5, 3–20, 1972.

[46] Mi Z, Li Q, Hu Y, Liu C, Qiao Y. “Fracture Properties of Concrete in Dry Environments with Different Curing Temperatures.” *Applied Sciences*. 2020.